The Journal of Physiology

Phosphatidylinositol 4,5-bisphosphate (PIP$_2$) modulates afterhyperpolarizations in oxytocin neurons of the supraoptic nucleus

Matthew K. Kirchner [iD], Robert C. Foehring, Lie Wang, Giri Kumar Chandaka, Joseph C. Callaway and William E. Armstrong

Department of Anatomy and Neurobiology and Neuroscience Institute, University of Tennessee Health Science Center, Memphis, TN, USA

Key points

- Afterhyperpolarizations (AHPs) generated by repetitive action potentials in supraoptic magnocellular neurons regulate repetitive firing and spike frequency adaptation but relatively little is known about PIP$_2$'s control of these AHPs.
- We examined how changes in PIP$_2$ levels affected AHPs, somatic $[Ca^{2+}]_i$, and whole cell Ca^{2+} currents.
- Manipulations of PIP$_2$ levels affected both medium and slow AHP currents in oxytocin (OT) neurons of the supraoptic nucleus.
- Manipulations of PIP$_2$ levels did not modulate AHPs by influencing Ca^{2+} release from IP$_3$-triggered Ca^{2+} stores, suggesting more direct modulation of channels by PIP$_2$.
- PIP$_2$ depletion reduced spike-evoked Ca^{2+} entry and voltage-gated Ca^{2+} currents.
- PIP$_2$ appears to influence AHPs in OT neurons by reducing Ca^{2+} influx during spiking.

Abstract Oxytocin (OT)- and vasopressin (VP)-secreting magnocellular neurons of the supraoptic nucleus (SON) display calcium-dependent afterhyperpolarizations (AHPs) following a train of action potentials that are critical to shaping the firing patterns of these cells. Previous work demonstrated that the lipid phosphatidylinositol 4,5-bisphosphate (PIP$_2$) enabled the slow AHP component (sAHP) in cortical pyramidal neurons. We investigated whether this phenomenon occurred in OT and VP neurons of the SON. Using whole cell recordings in coronal hypothalamic slices from adult female rats, we demonstrated that inhibition of PIP$_2$ synthesis with wortmannin robustly blocked both the medium and slow AHP currents (I_{mAHP} and I_{sAHP}) of OT, but not VP neurons with high affinity. We further tested this by introducing a water-soluble PIP$_2$ analogue (diC$_8$-PIP$_2$) into neurons, which in OT neurons not only prevented wortmannin's inhibitory effect, but slowed rundown of the I_{mAHP} and I_{sAHP}. Inhibition of phospholipase C (PLC) with U73122 did not inhibit either I_{mAHP} or I_{sAHP} in OT neurons, consistent with wortmannin's effects not being due to reducing diacylglycerol (DAG) or IP$_3$ availability, i.e. PIP$_2$ modulation of AHPs is not likely to involve downstream Ca^{2+} release from inositol 1,4,5-trisphosphate (IP$_3$)-triggered Ca^{2+}-store release, or channel modulation via DAG and protein kinase C (PKC). We found that wortmannin reduced $[Ca^{2+}]_i$ increase induced by spike trains in OT neurons, but had no effect on AHPs evoked by uncaging intracellular Ca^{2+}. Finally, wortmannin selectively reduced whole cell Ca^{2+} currents in OT neurons while leaving VP neurons unaffected. The results indicate that PIP$_2$ modulates both the I_{mAHP} and I_{sAHP} in OT neurons, most likely by controlling Ca^{2+} entry through voltage-gated Ca^{2+} channels opened during spike trains.

Abbreviations   AHP, afterhyperpolarization; DAG, diacylglycerol; I_{AHP}, afterhyperpolarization current; MNC, magnocellular neurosecretory cell; OT, oxytocin; PKC, protein kinase C; PLC, phospholipase C; PVN, paraventricular nucleus; SON, supraoptic nucleus; VP, vasopressin.

Introduction

Oxytocin (OT)- and vasopressin (VP)-secreting magnocellular neurosecretory cells (MNCs) play a crucial role in many physiological functions including lactation, parturition (OT cells) and cardiovascular regulation (VP cells) (Armstrong *et al.* 2010). The release of both hormones is optimized by a burst-firing pattern of action potentials, albeit of different form in the two cell types (Dutton & Dyball, 1979; Bicknell & Leng, 1981; Cazalis *et al.* 1985). Sustained stimulation of these cells (most notably VP) results in significant reduction of hormone release over time, whereas periods of quiescence reverse this secretory fatigue (Bicknell, 1988). Furthermore, the burst-firing is synchronized among all OT neurons in the supraoptic nucleus (SON) and paraventricular nucleus (PVN) (Belin *et al.* 1984) during lactation, whereas VP neurons burst asynchronously (Sabatier & Leng, 2007). Many cell types, including MNCs, express calcium-activated potassium currents that (i) produce afterhyperpolarizations (AHPs) following a single action potential or train of action potentials and (ii) shape firing patterns. In MNCS, the AHP typically comprises three components with varying time courses mediated by different channels: fast (fAHP), medium (mAHP), and slow (sAHP). The fast AHP current (I_{fAHP}) is contributed by $K_{Ca}1.1$ (BK) channels as well as voltage-gated K^+ channels, and lasts <15 ms (Dopico *et al.* 1999; Hlubek & Cobbett, 2000; Roper *et al.* 2003). The medium AHP current (I_{mAHP}) lasts ∼500 ms, is underlain by $K_{Ca}2.3$ (SK3) channels (Stocker & Pedarzani, 2000; Tacconi *et al.* 2001), and is blocked by apamin (Bourque & Brown, 1987). The channel underlying the slow AHP current (I_{sAHP}) in MNCS (and most neuron types) is unknown, but is Ca^{2+} dependent and lasts on the order of seconds (Ghamari-Langroudi & Bourque, 2004; Andrade *et al.* 2012). Pinpointing an exact mechanism underlying the sAHP has been difficult because the I_{sAHP} characteristics differ among neuronal cell types (Andrade *et al.* 2012). However, there are some common features, including activation by rises in $[Ca^{2+}]_i$, modulation by neurotransmitters, and voltage independence. This gap in our understanding is important because the I_{sAHP} controls spike frequency adaptation and is affected by major intracellular signals, including Ca^{2+}, in many cell types of several brain regions. With regard to MNCs, the I_{mAHP} and I_{sAHP} are of particular interest due to their significant influence on burst firing patterns. Further, the AHPs in OT neurons get larger during late pregnancy and lactation (Stern & Armstrong, 1996; Teruyama & Armstrong, 2002), coinciding with an increase in pulsatile OT release from the neurohypophysis during labour and lactation (Wakerly & Lincoln, 1971; Higuchi *et al.* 1986) and the adoption of synchronized bursting firing patterns (Poulain & Wakerley, 1982).

While we do not know how Ca^{2+} activates the unknown AHP channels, a study in neocortical pyramidal cells demonstrated that phosphatidylinositol 4,5-bisphosphate (PIP_2) facilitates the I_{sAHP} but not the SK-mediated I_{mAHP} (Villalobos *et al.* 2011). This is intriguing because PIP_2 is known to influence the properties of a host of channel types and is activated by G_q-coupled receptors (Hille, 1994; Suh & Hille, 2002, 2008; Suh *et al.* 2010; Kruse & Hille, 2013), including receptors that are activated by neurotransmitters known to attenuate the I_{sAHP}, (e.g. acetylcholine via muscarinic receptors). These features, combined with the slow current kinetics and strong Ca^{2+} dependence, support the hypothesis that a biochemical signalling cascade contributes to modulation of the I_{sAHP}, which may influence more than one channel type (Andrade *et al.* 2012).

Methods

Ethical approval

These studies were performed on virgin adult Sprague-Dawley female rats (Harlan Laboratories, Indianapolis, IN, USA) weighing between 150–220 g. The UTHSC IACUC review board approved all experiments and the experiments conform to the principles of UK regulations as described in (Drummond, 2009). Animals were on an *ad libitum* diet. For use in experiments, rats were deeply anesthetized with either sodium pentobarbital (100 mg kg^{-1}) or ketamine–xylazine (10% xylasine; 100 mg kg^{-1}) and perfused through the heart with artificial cerebrospinal fluid (aCSF) with NaCl replaced by 210 mM sucrose. The rats were decapitated via guillotine. The brains were then removed and subsequently sliced for use in whole cell patch clamp electrophysiology. The work described in this report complies with ethical standards and protocols under which *The Journal of Physiology* operates as described in Grundy (2015). AHPs in OT neurons undergo significant plastic changes during the female reproductive cycle (Teruyama & Armstrong, 2002, 2005). Because of this, we limit our study to females because these changes offer insights into the MNC-specific mechanisms of AHP generation.

Slice preparation

Coronal brain slices 250 μm thick were cut in ice-cold aCSF with 210 mM sucrose replacing NaCl, using a Leica VT1000S vibratome. After cutting, the brain slices were transferred to an aCSF-filled holding chamber and warmed for 15–20 min at 32°C. aCSF was continuously bubbled with 95% O$_2$–5% CO$_2$, and contained (in mM): 20 D-glucose, 0.45 ascorbic acid, 2.5 KCl, 1 MgSO$_4$, 1.25 NaH$_2$PO$_4$.H$_2$O, 26 NaHCO$_3$, 125 NaCl, 2 CaCl$_2$. Slices were then transferred to aCSF at room temperature, where they remained for at least 40 min prior to recording.

Electrophysiology

Slices were placed in the well of a Plexiglass chamber attached to a modified stage on an Olympus BX51WI upright microscope and perfused with aCSF containing 5 mM CsCl to block the slow depolarizing after-potential (sDAP) (Ghamari-Langroudi & Bourque, 1998; Teruyama & Armstrong, 2005, 2007). The aCSF was bubbled constantly with 95% O$_2$–5% CO$_2$, warmed to 32°C $\pm$ 1°C, and flowed at ~2 ml min^{-1}. Whole cell voltage clamp recordings were obtained using an Axon Multiclamp 700B amplifier (Molecular Devices, Sunnyvale, CA, USA). Traces were digitized using an Axon 1440A Digitizer at 10 kHz and filtered at 2 kHz on a Dell desktop computer running Clampex 9 software (Molecular Devices).

Recording pipettes (4–8 MΩ) were pulled from borosilicate glass with an outer diameter of 1.5 mm using a P-1000 flaming/brown horizontal micropipette puller (Sutter Instruments, Sovato, CA, USA). The pipette internal solution for analysing AHP tail currents consisted of (in mM): 135 KMeSO$_4$, 8 NaCl, 10 Hepes, 2 Mg-ATP, 0.3 Na-GTP, 0.1 leupeptin, 6 phosphocreatine, 0.2 EGTA with pH 7.2–7.4 and 285–295 mosmol (kg H$_2$O)$^{-1}$. 0.1% biocytin (Sigma-Aldrich, USA) was added to an aliquot on the day of the experiment for visualization during immunochemical identification of cell type. The liquid junction potential for the KMeSO$_4$ internal was ~-10 mV, and was not corrected. For certain experiments, 30 μM diC$_8$-PIP$_2$ (Echelon Biosciences, Salt Lake City, UT, USA) reconstituted in H$_2$O was added to the internal solution.

I_{AHP} tail currents were evoked using a voltage clamp protocol of a 17 spike, 5 ms pulse train at 20 Hz from a holding potential of -60 mV to $+20$ mV; the I_{AHP} was clamped at -60 mV immediately following the train. This was done to mimic a train of action potentials, and at 20 Hz, 17 spikes produced an I_{AHP} amplitude near maximum in pilot experiments (data not shown). In MNCs I_{AHP} amplitude correlates with spike count (Ghamari-Langroudi & Bourque, 2004).

Baseline I_{AHP} recordings were taken in the presence of 10 μM 6,7-dinitroquinoxaline-2,3-dione (DNQX), 40 μM 2R)-amino-5-phosphonovaleric acid (AP5), and 100 μM picrotoxin to block fast synaptic currents. Experimental reagents include 0.001–10 μM wortmannin (Sigma-Aldrich), 100 nM apamin (Sigma-Aldrich), 10 μM 2-(4-morpholinyl)-8-phenyl-4H-1-benzopyran-4-one (LY294,002) (Sigma-Aldrich) to block PI3K, 10 μM 1-[6-[[(17β)-3-methoxyestra-1,3,5(10)-trien-17-yl]amino]hexyl]-1H-pyrrole-2,5-dione (U73122) (Sigma-Aldrich) to block PLC, and 300 μM (cells were incubated before the experiment in 1 mM) myo-inositol (Sigma-Aldrich) (Villalobos *et al.* 2011) to supplement the substrate for PIP$_2$ production. Cells whose series resistance exceeded 20 MΩ and/or changed by more than 20% during the recording were discarded. I_{AHPs} were averaged over 2 or more runs.

For measuring whole cell Ca^{2+} currents, the external bath solution contained (in mM): 80 NaCl, 50 TEA-Cl, 5 CsCl, 1 MgCl$_2$, 10 Hepes, 10 glucose, 0.0005 tetrodotoxin (TTX), 0.1 picrotoxin, 4 CaCl$_2$. The pipette internal solution contained: 180 N-methyl-D-glucamine, 4 MgCl$_2$, 40 Hepes, 10 EGTA, 12 phosphocreatine, 2 Mg-ATP, 0.4 Na-GTP. The liquid junction potential for this internal solution is ~-5 mV and was not corrected. Cells were held at -70 mV. For *I–V* curves, cells were hyperpolarized to -90 mV for 200 ms followed by 10 mV 1000 ms steps up to $+10$ mV. Cd^{2+} at 400 μM was bath-applied at the end of each trial to confirm the Ca^{2+} current. *I–V* curves were derived from the steady-state measurement of these steps. Currents were leak subtracted by scaling the current in response to a $+10$ mV step from baseline.

Immunochemistry

Slices were fixed in 4% paraformaldehyde and 0.2% picric acid in phosphate buffered saline (PBS) and stored at 4°C post-experimentally. Biocytin-labelled neurons were processed for double labelling with either anti-OT- or VP-neurophysins. The anti-VP-neurophysin is a rabbit polyclonal antibody provided by Alan Robinson (UCLA, Emeritus), and was used at 1:20,000. The anti-OT-neurophysin antibody (PS36) is a mouse monoclonal antibody provided by Harold Gainer (National Institutes of Health, Emeritus) and was used at 1:500. All antibodies and labelling reagents were dissolved in PBS + 0.5% Triton X-100 (PBST). After 36–72 h of incubation at 4°C, the slices were washed with PBST and incubated in a cocktail of secondary antibodies including Alexa Fluor 488 goat anti-rabbit immunoglobulin G (IgG) and Alexa Fluor 594 goat anti-mouse IgG (1:200) along with Avidin-AMCA (1:200) for reaction with the biocytin. Double staining of biocytin and one antibody complemented with the negative staining of the other identified neurons as OT or VP (Fig. 1).

Calcium imaging and uncaging

Electrophysiology and Ca^{2+} imaging were performed simultaneously on a single computer using a custom windows-based program (CCD32; written by Dr J. Callaway, UTHSC, Memphis, TN, USA, based on software developed by Lasser-Ross *et al.* (1991). Voltage clamp recordings were acquired using an Axopatch 700A (Molecular Devices, Sunnyvale, CA, USA). Electrodes were pulled using borosilicate electrodes (4–8 MΩ). The pipette internal solution for analysing AHP tail currents was as previously described, except with 0.2 mM EGTA replaced with 0.1 mM fura-2. Images were obtained with a CCD Imago Sensicam camera, using a Polychrome V monochromater (TILL Photonics, Planegg, Germany) to control excitation wavelength and intensity. Calcium fluorescence was obtained by exciting fura-2 at 380 nm using a USHIO UXL-150MO 150 W xenon arc lamp. We measured fluorescence changes at an emission wavelength of 520 ± 40 nm. Photobleaching was corrected by subtracting a Ca^{2+} signal from a control sweep at equal length, in which the cell was not stimulated and held at a hyperpolarized holding potential (-70 mV) to minimize Ca^{2+} entry. We subtracted background autofluorescence by using a reference area near the cell. Measurements were made from the soma, excluding the nucleus.

To uncage Ca^{2+}, we used 2 mM DM-nitrophen as the Ca^{2+} caging compound loaded into the internal solution with 40% calcium occupancy (0.8 mM $CaCl_2$). In the internal solution, 0.2 mM EGTA was replaced with 0.05 mM fluo-4 for Ca^{2+} imaging. Fluo-4 was excited at 488 nM and measured at 520 ± 40 nm. Additionally, Mg-ATP was replaced by Na-ATP to avoid loading the caging compound with Mg^{2+}. We used a xenon flashlamp (Rapp Optoelectronic, JML-C2) for photolysis and discharged 72.6 J in ~1 ms with UV light. Upon photolysis, the K_d of DM-nitrophen for Ca^{2+} increases from 5 nM to 3 mM, rapidly releasing Ca^{2+} into the cell (Sah & Clements, 1999).

All Ca^{2+} imaging data are reported as percentage relative change in fura-2 fluorescence (%$\Delta F/F$). These data were analysed either with the custom acquisition program described above, or with Igor Pro 7.0 (Wavemetrics Inc., Portland, OR, USA).

Dissociated cells and PIP$_2$ distribution

Adult female rats (150–220 g) ($n = 5$) were anaesthetized with ketamine–xylasine (dose) and perfused through the heart with cold sucrose solution as described above for slices. We adapted the protocol of Shah *et al.* (2014) for assessing PIP$_2$ labelling in dissociated SON neurons. Tissue blocks from the SON area were excised from 200 μm sections taken with a vibratome, and incubated in oxygenated Pipes (in mM: 110 NaCl, 5 KCl, 1 $MgCl_2$, 1 $CaCl_2$, 20 Pipes and 25 glucose, pH 7.1, containing trypsin (0.6 mg ml^{-1}; Sigma Aldrich) for 90 min at 34°C. The tissue was transferred to oxygenated Pipes without trypsin for 30 min at room temperature, then gently triturated with three different sizes of fire-polished pasture pipettes. The cells were plated into two wells from a 6-well plate (Cat. P06-1.5H-N, In Vitro Scientific, Sunnyvale, CA, USA) and allowed to settle at room temperature for 30 min. One well was then treated with 100 nM wortmannin in Pipes for 30 min at room temperature, while the second well was untreated. The media in each well was then replaced with fixative (4% paraformaldehyde with 0.2% picric acid in 0.01 M PBS) and incubated overnight at 4°C. The fixative was rinsed 3× with PBS and the cells then treated with 10% non-fat dry milk in PBS for 1 h at room temperature to block non-specific antibody interactions. The cells were incubated overnight at 4°C for double labelling with an antibody raised in rabbit against OT–NP (oxytocin–neurophysin, 1:5000) + mouse anti-PIP$_2$ antibody (1:1000, Cat. ADI-915-062-100, Enzo Life Sciences), rinsed 3× in PBS then incubated in a cocktail of secondary antibodies for 1 h at room temperature. The secondary antibodies used were goat-anti-rabbit (Alexa Fluor 568 nm, Invitrogen, Carlsbad, CA, USA) and goat-anti-mouse (Alexa Flour 488 nm, Invitrogen)
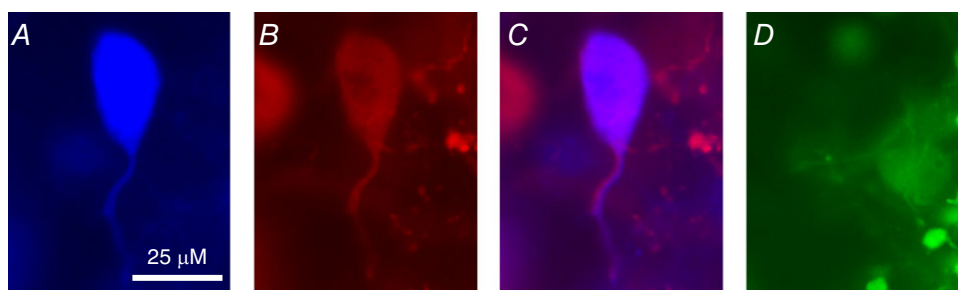

Figure 1. An example of a positively identified OT cell using immunolabelling
A, a single cell loaded with biocytin during recording, and subsequently labelled with Avid-AMCA. The tissue was then labelled for OT- and VP-neurophysins (NP) by double immunofluorescence using Alexa Fluor 594- and Alexa Fluor 488-conjugated antibodies, respectively. This biocytin-labelled cell was immunoreactive to the OT-NP (*B* and *C*) but not to VP-NP (*D*).

conjugated IgGs at 1:200 dilutions with PBS. Cells were rinsed 3× in PBS then stained with DAPI (300 nM, Cat. D9542, Sigma Aldrich) in PBS for 5 min. Cells were rinsed 3× in PBS and left immersed in PBS for microscopic analysis.

Images were acquired with a Zeiss 710 confocal inverted microscope (Carl Zeiss Microscopy, Thornwood, NY, USA) using a 63× oil-immersion objective (n.a. 1.4). OT-positive neurons were located and 1 μm optical sections were collected from the top to the bottom of each cell sampled. The laser power (18%) and the pin-hole (2.5 AU) were constant for all the images taken and well below saturation. Only cells that were positive for both OT–NP and PIP$_2$ antibodies as well as exhibiting clear DAPI nuclear staining were considered for the study. For each group, from each animal, at least 31 images were taken. Thus a total of more than 150 cells per group (control and wortmannin treated) were analysed for this study. Data were analysed blind. One investigator made the dissociated cell preparation, drug treatment and anti-body staining. A second investigator acquired the images blind to the two groups, then coded the digital images for measurements by the first investigator. Thereafter the second investigator decoded the cells, and the first investigator made the appropriate statistical analysis.

Images were analysed with Image J (NIH, Bethesda, MD, USA). Each Z-stack had between 15 and 25 optical sections, thus a PIP$_2$ image for analysis was selected from each cell based on the maximum size of the nucleus through the stack. For measuring the average membrane (or near membrane) intensity of PIP$_2$ staining for each cell, the line tool with freehand line option was used to draw a line (5 pixels) around the edge of the cell and the mean pixel intensity value was recorded. To measure the average intensity of the cytoplasm, an area excluding the nucleus and the perimeter of the cell was selected using the polygon tool (1 pixel), and the mean intensity was recorded. Such mean intensities recorded were then subtracted from the mean background intensity for each cell. To measure mean background intensity from each cell, a uniform dark spot was selected using the polygon tool (1 pixel), and the mean intensity was recorded. The data are presented as cytoplasm: membrane ratios. These ratios were then averaged for each group in each animal, and analysed with a Wilcoxon ranked-sum non-parametric test, using JMP Pro 12.

Statistics and analysis

In MNCs the I_{fAHP} is a fast, transient event lasting <15 ms (Dopico *et al.* 1999), and was not evaluated herein. The I_{mAHP} decay tau is ∼500 ms in MNCs (Teruyama & Armstrong, 2005), whereas the I_{sAHP} has a decay tau of 1–2 s in MNCs (Ghamari-Langroudi & Bourque, 2004). With this consideration, we operationally defined the I_{mAHP} and I_{sAHP} as the amplitude of the AHP tail current (I_{AHP}) at 100 ms and 1000 ms after the stimulus, respectively. While measurement of the I_{mAHP} at 100 ms is likely to contain a small contribution from the I_{sAHP}, it is dominated by the I_{mAHP} due to the slower onset kinetics of the I_{sAHP} (Teruyama & Armstrong, 2005). Furthermore, we demonstrate in the Results section that the SK channel blocker apamin (100 nM) inhibits the I_{mAHP} by 70.5 ± 5.5% (data not shown). In some experiments, the I_{sAHP} was selectively evaluated after isolation in the presence of 100 nM apamin.

All electrophysiological traces were analysed in ClampFit 10.2 (Molecular Devices) or Igor Pro. Because the I_{mAHP} and I_{sAHP} are relatively small currents, special considerations were taken when measuring them in voltage clamp. During analysis, the currents were further filtered using a Gaussian lowpass filter at 1 kHz. Measurements of amplitude were averaged over a 30 ms segment of current (30 points). This was done to marginalize the contribution of electrical noise to individual points. All statistics were performed in SPSS. Unless stated otherwise, data were compared using a Student's paired samples *t* test. For the experiment comparing controls to apamin and apamin + wortmannin (Fig. 5), we ran a repeated measures ANOVA with a Bonferroni *post hoc* test for pairwise comparisons. All reported values are represented as means ± SEM.

Results

Depleting PIP$_2$ from cells inhibits the I_{mAHP} and I_{sAHP} of OT but not VP neurons

Previous work demonstrated that PIP$_2$ levels are critical for generation of I_{sAHP}, but not I_{mAHP}, in cortical pyramidal neurons (Villalobos *et al.* 2011). To test this in SON neurons, we bath-applied wortmannin and measured the macroscopic AHP tail current (I_{AHP}) at two time points (see Methods section: Data and analysis). Wortmannin is a pharmacological agent known to inhibit PIP$_2$ levels by blocking the rate-limiting enzyme of PIP$_2$ production, PI4Kα (Nakanishi *et al.* 1995) (Fig. 2). Application of wortmannin (10 μM) caused a significant decrease in both I_{mAHP} and I_{sAHP} of OT supraoptic neurons ($n = 10$, $P < 0.001$; 100 ms: control 22.12 ± 1.9 pA *vs.* wortmannin 2.67 ± 0.3 pA; 1000 ms: control 6.48 ± 0.9 pA *vs.* wortmannin 1.01 ± 0.4 pA; Fig. 3). In contrast to OT cells, VP cells demonstrated no significant change in I_{mAHP} and I_{sAHP} in response to wortmannin ($n = 9$, $P > 0.05$; 100 ms: control 19.67 ± 4.2 pA *vs.* wortmannin 23.72 ± 5.1 pA; 1000 ms: control 5.44 ± 1 pA *vs.* wortmannin 6.12 ± 1.1 pA; Fig. 3). To characterize wortmannin's effect on AHPs further, we generated a dose–response curve measuring percentage of I_{mAHP} inhibition as a function of wortmannin concentration.

We used the I_{mAHP} time point because current amplitudes were much larger, allowing clear measurements at all doses. Wortmannin's effects on OT neurons were dose dependent, characterized by a sigmoidal dose–response relationship with an $IC_{50} = 58$ nM and a Hill coefficient of 1.6 (Fig. 3*D*). This indicates that wortmannin exhibits specific effects at nanomolar concentrations, with non-cooperative binding. While the effect of wortmannin was similarly dose dependent on the I_{sAHP}, with stronger inhibition at increased wortmannin concentrations, dose–response plots could not be reliably fitted with a Hill equation due to the small amplitude of the I_{sAHP} (≤ 20 pA; data not shown).

Although wortmannin is an inhibitor of PIP_2 synthesis, it also depletes PIP_3 by inhibiting phosphoinositide 3-kinase (PI3K) (Meyers & Cantley, 1997; Vanhaesebroeck

et al. 2001). Furthermore, PI3K is the higher affinity target in comparison to PI4Kα (Meyers & Cantley, 1997; Vanhaesebroeck *et al.* 2001). We thus bath-applied the specific PI3K inhibitor LY294,002 (10 μM: Vlahos *et al.* 1994; Lee *et al.* 2007; Wang *et al.* 2016) to both OT and VP neurons to test for PIP_3 involvement. This control has been used previously in studies of PIP_2-affected AHPs in cortex (Villalobos *et al.* 2011). As in pyramidal neurons, LY294,002 had no significant effect on the I_{mAHP} or I_{sAHP} of either cell type (OT: $n = 7$, $P > 0.05$; control 46.1 ± 6.4 pA *vs.* wortmannin 44.18 ± 7.4 pA; VP: $n = 4$, $P > 0.05$; control 36.48 ± 10.4 pA *vs.* wortmannin 38.58 ± 10.5 pA; Fig. 4), consistent with wortmannin reducing the AHPs by its action on PI4Kα.

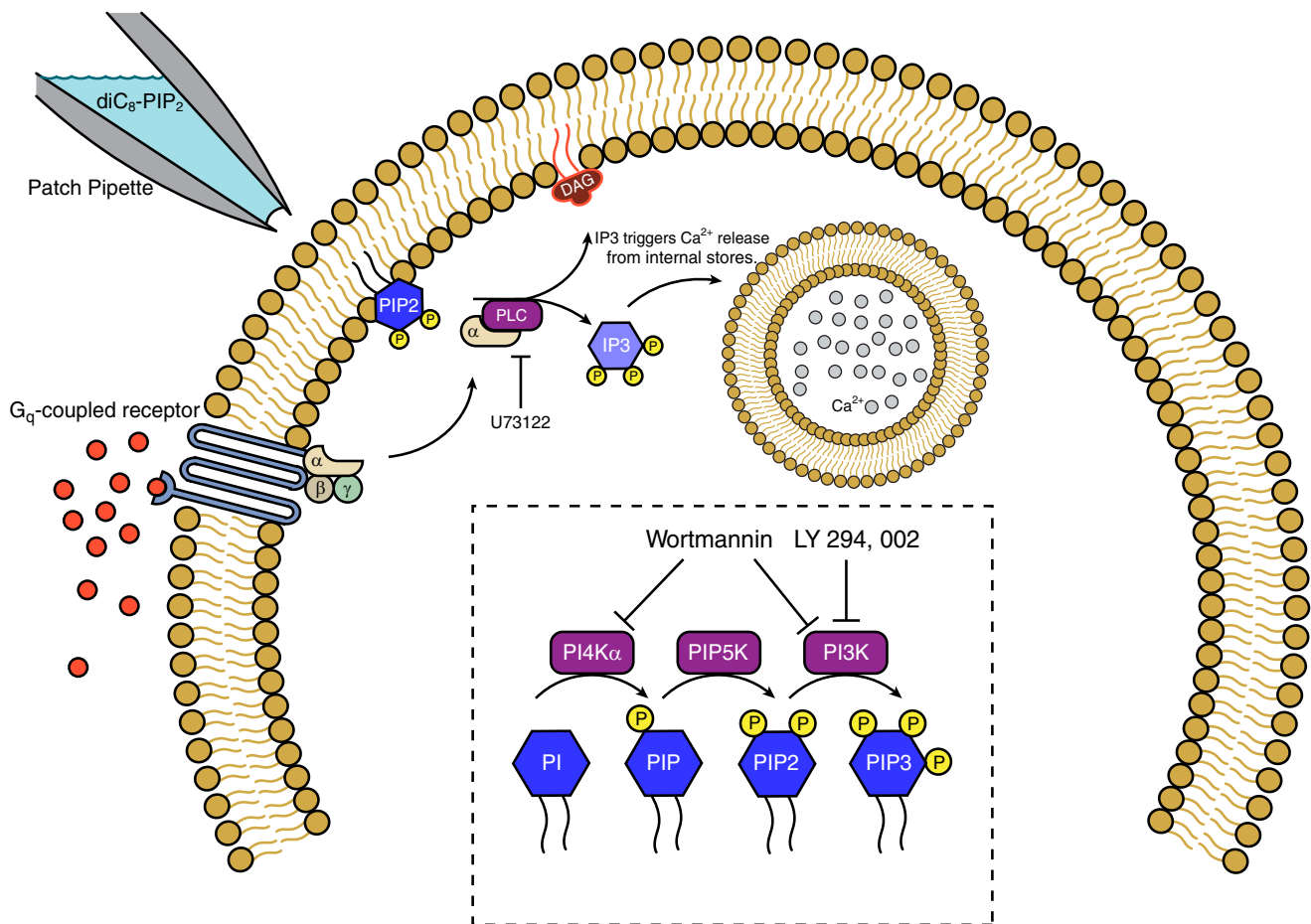To ensure that wortmannin's effects reflected a response specific to AHPs and not a change in general cell health,

Figure 2. Diagram of the relevant PIP$_2$ pathways
Upon stimulation of G$_q$-coupled receptors, the α component of the G-protein activates phospholipase-C (PLC), which cleaves membrane-bound PIP$_2$ into diacylglycerol (DAG) and inositol trisphosphate (IP$_3$). DAG activates protein kinase C while IP$_3$ triggers release of Ca^{2+} ions from internal Ca^{2+} stores. U73122 blocks the activity of PLC. PIP$_2$ has been demonstrated to modulate several ion channels in previous studies, such as Kv7 channels (Suh & Hille, 2007) and SK channels (Zhang *et al.* 2014). Inset, the dashed box displays the pathway for production of different PIP molecules (blue hexagons), and the enzymes that phosphorylate each of them (purple boxes). Wortmannin blocks synthesis of PIP$_2$ and PIP$_3$ production while LY294,002 only blocks PIP$_3$ production. Both work by blocking the synthetic enzymes.

10 MNCs (5 OT and 5 VP) were assessed in current clamp recordings, where we found no significant differences in spike amplitude (OT: $P > 0.05$; 61.5 ± 2.8 mV control vs. 59.2 ± 3.2 mV wortmannin; VP: $P > 0.05$; 65.6 ± 4.0 mV control vs. 65.0 ± 3.8 mV wortmannin), spike half-width (OT: $P > 0.05$; 2.3 ± 0.1 ms control vs. 2.5 ± 0.1 ms wortmannin; VP: $P > 0.05$; 2.5 ± 0.1 ms control vs. 2.4 ± 0.1 ms wortmannin), resting membrane potential (OT: $P > 0.05$; −60.0 ± 0.6 mV control vs. −60.2 ± 0.7 mV wortmannin; VP: $P > 0.05$; −58.9 ± 2.6 mV control vs. −60.6 ± 2.2 mV wortmannin), or input resistance (OT: $P > 0.05$; 467.37 ± 57.5 MΩ control vs. 444.49 ± 55.3 MΩ wortmannin; VP: $P > 0.05$; 545.75 ± 110.8 MΩ control vs. 528 ± 107.3 MΩ wortmannin) in cells before and after wortmannin application.

Wortmannin inhibits the I_{sAHP} in the presence of apamin in OT neurons

To isolate wortmannin's effects on the sAHP, we tested its effects in the presence of apamin, which blocks SK channels and thus the I_{mAHP} in MNCs (Bourque & Brown, 1987; Erickson et al. 1993; Armstrong et al. 1994; Kirkpatrick & Bourque, 1996; Teruyama & Armstrong, 2005). Since we bath-applied apamin (100 nM) first, followed by the addition of wortmannin (1 μM), we first ran a repeated measures ANOVA that revealed a significant main effect ($P < 0.001$). Post hoc analysis found that in OT neurons, apamin resulted in robust (∼70%) inhibition of the I_{mAHP} (measured at 100 ms: $n = 7$, $P < 0.001$; control 18.76 ± 2.5 pA vs. apamin 6.14 ± 1.8 pA; Fig. 5) while
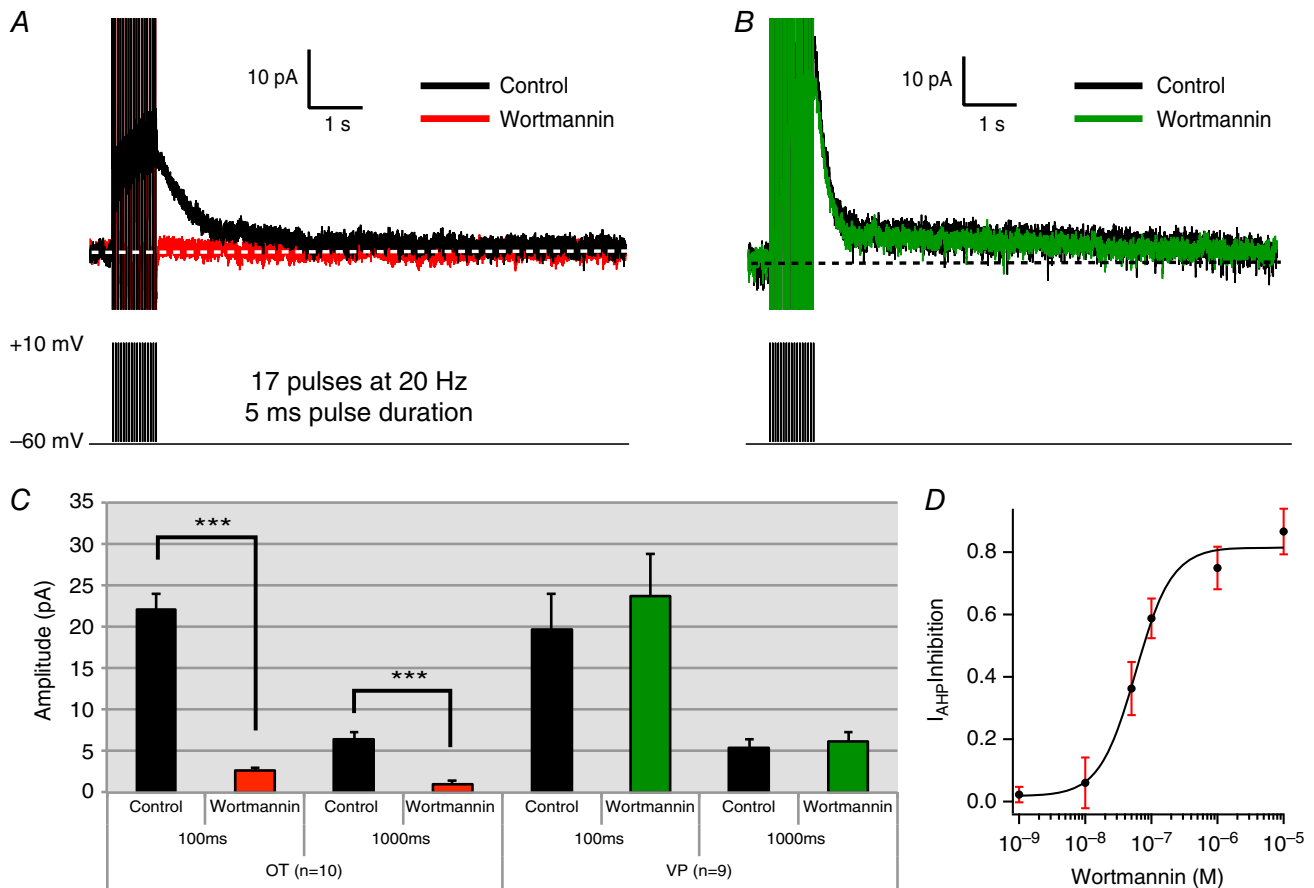

Figure 3. Wortmannin (10 μm), a PIP$_2$ and PIP$_3$ inhibitor, blocks the I_{mAHP} and I_{sAHP} of OT neurons but not VP neurons

A and B, voltage clamp recording of a supraoptic magnocellular OT (A) and VP (B) cell before and after wortmannin application. Wortmannin application inhibits both the I_{mAHP} and I_{sAHP} in OT cells while having no effect in VP cells. C, summary data of the wortmannin effect on OT and VP cells: I_{AHP} amplitude was measured at 100 ms (I_{mAHP}) and 1000 ms (I_{sAHP}) after the end of the pulse. OT cells demonstrate statistically significant inhibition of both the I_{mAHP} and I_{sAHP} ($n = 10$, ***$P < .001$). In contrast, VP cells demonstrate no significant change in I_{mAHP} or I_{sAHP} amplitude ($n = 9$, $P > 0.05$). D, dose–response curve for wortmannin in OT neurons. We plotted peak I_{mAHP} inhibition as a function of wortmannin concentration. Wortmannin exerted robust inhibition at nanomolar concentrations (IC$_{50}$ = 58 nM). The Hill Coefficient of 1.6 ± 0.02 indicates relatively non-cooperative binding. A minimum of 5 cells was collected for each concentration of wortmannin. [Colour figure can be viewed at wileyonlinelibrary.com]

having no effect on the I_{sAHP} (measured at 1 s: $n = 7$, $P > 0.05$; control 6.70 ± 1.5 pA *vs.* apamin 6.10 ± 1.4 pA; Fig. 5). Application of wortmannin inhibited the I_{sAHP} in the presence of apamin (measured at 1 s: $n = 7$, $P < 0.05$; apamin 6.10 ± 1.4 pA *vs.* wortmannin + apamin 2.81 ± 0.8 pA; Fig. 5). We also observed further inhibition of the I_{AHP} at 100 ms ($n = 7$, $P < 0.05$; apamin 6.14 ± 1.8 pA *vs.* wortmannin + apamin 1.2 ± 0.4 pA; Fig. 5). For comparison, wortmannin had no effect on apamin-treated VP neurons (measured at 1 s: $n = 6$, $P > 0.05$; apamin 6.79 ± 1.6 pA *vs.* wortmannin + apamin 6.23 ± 1.9 pA). These data confirm that wortmannin acts on the isolated I_{sAHP} in addition to I_{mAHP} in OT cells.

Wortmannin reduced PIP$_2$ immunoreactivity in OT neurons

To determine whether the application of wortmannin at a similar dose to our electrophysiological experiments was associated with changes in the cellular distribution of PIP$_2$ in OT neurons, we calculated the ratio of the staining intensity of PIP$_2$ immunoreactivity of the cytoplasm *vs.* membrane in dissociated cell preparations and compared control neurons with those exposed to 100 nM wortmannin ($n = 5$ animals in each group). As shown in Fig. 6, this ratio was significantly increased by wortmannin, suggesting depletion of membrane PIP$_2$. This type of redistribution is similar to that reported for PIP$_2$ in response to muscarinic modulation in sympathetic neurons (Suh & Hille, 2002; Delmas & Brown, 2005).

diC$_8$-PIP$_2$ in the pipette prevents I_{mAHP} and I_{sAHP} inhibition by wortmannin

We have shown that application of wortmannin blocks both the medium and slow I_{AHPs} in OT neurons. We interpret this as wortmannin blocking PIP$_2$ synthesis and thus reducing total PIP$_2$ levels. In contrast, wortmannin has no significant effect on these I_{AHPs} in VP neurons. We next tested whether directly increasing the amount of available PIP$_2$ inside the cell affected AHPs and whether
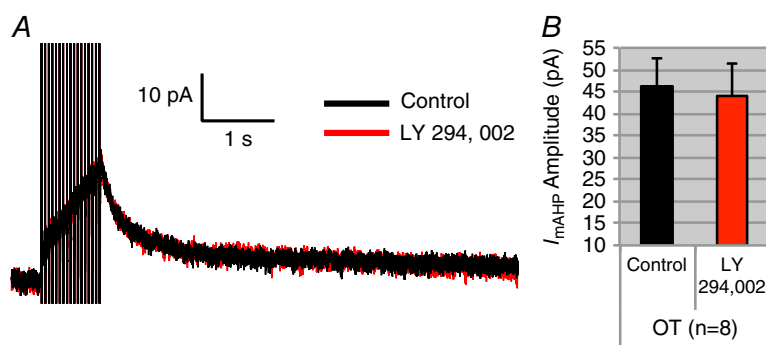

Figure 4. LY294,002 has no effect on the I_{AHP}
Because wortmannin also blocks PIP$_3$, we tested the selective PIP$_3$ blocker LY294,002 on the I_{AHP}. *A*, an example of LY294,002's effect on an OT neuron. *B*, summary data of I_{mAHP} amplitude in OT neurons. There was no significant difference ($n = 8$, $P > 0.05$). [Colour figure can be viewed at wileyonlinelibrary.com]
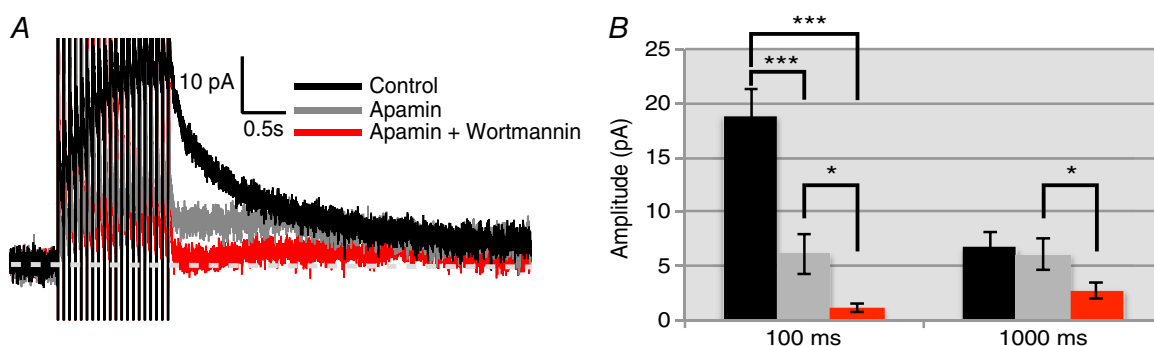

Figure 5. Wortmannin inhibits the apamin-treated I_{AHP} in OT neurons while having no effect in VP neurons
Apamin (100 nM) was applied to MNCs to block the I_{mAHP} in both cell types, followed by wortmannin (1 μM) to observe effects on the isolated I_{sAHP}. *A*, voltage clamp trace of I_{AHP} from an OT neuron. This contains a baseline recording (black trace), apamin treated trace to block the I_{mAHP} (grey), and a trace with apamin and wortmannin (red). Wortmannin inhibited the apamin-isolated I_{sAHP}. *B*, summary data of OT ($n = 6$) neurons. There was a significant main effect (repeated measures ANOVA, $F_{(2,12)} = 45.97$, ***$P < 0.001$). Apamin inhibits the I_{mAHP} at 100 ms (***$P < 0.001$). Measurements of the I_{sAHP} (1000 ms) indicate that apamin has little effect at this time, while subsequent wortmannin application significantly reduces the isolated I_{sAHP} (*$P < 0.05$). [Colour figure can be viewed at wileyonlinelibrary.com]

it prevented the inhibition by wortmannin. We supplied the water-soluble PIP$_2$ analogue diC$_8$-PIP$_2$ (30 μM) into neurons through the patch pipette to provide a constant source of PIP$_2$. Wortmannin had no significant effect on I_{mAHP} and I_{sAHP} in OT neurons when diC$_8$-PIP$_2$ was dialysed into the cell (100 ms: $n = 8$, $P > 0.05$; diC$_8$-PIP$_2$ 17.62 $\pm$ 1.9 pA $vs.$ diC$_8$-PIP$_2$ + wortmannin 15.18 $\pm$ 2.4 pA; 1000 ms: $n = 8$, $P > 0.05$; diC$_8$-PIP$_2$ 4.13 $\pm$ 0.8 pA $vs.$ diC$_8$-PIP$_2$ + wortmannin 3.82 $\pm$ 1 pA; Fig. 7).

Supplying the PIP$_2$ precursor myo-inositol also prevents inhibition by wortmannin

Another means of saturating the PIP$_2$ supply is by adding the obligatory precursor myo-inositol in the bath. Myo-inositol is actively transported into the cell and increases PIP$_2$ production (Fisher *et al.* 1992, 2002; Villalobos *et al.* 2011). We pre-incubated slices in aCSF in 1 mM myo-inositol for 1 h. For recording, slices were then transferred to a solution of 300 μM myo-inositol in aCSF. Wortmannin (1 μM) had no effect on OT AHPs in the presence of myo-inositol (100 ms: $n = 7$, $P > 0.05$; myo-inositol 14.03 $\pm$ 1.6 pA $vs.$ myo-inositol + wortmannin 14.27 $\pm$ 1.5 pA; 1000 ms: $n = 7$, $P > 0.05$; myo-inositol 4.11 $\pm$ 0.8 pA $vs.$ myo-inositol + wortmannin 4.49 $\pm$ 0.6 pA; Fig. 8), similar to the results with diC$_8$-PIP$_2$ in the pipette (Fig. 7).

diC$_8$-PIP$_2$ slows rundown of the I_{mAHP} in OT neurons

Rundown is a term used to describe the decreased amplitude of I_{AHPs} over long recording sessions (Fig. 9A).

Since a previous study in neocortical pyramidal neurons showed that enhancement or inhibition of PIP$_2$ slows or hastens the rundown of the sAHP, respectively (Villalobos *et al.* 2011), we supplied the cells with water-soluble diC$_8$-PIP$_2$ (30 μM), and then evaluated rundown of the peak I_{AHP} in cells with or without diC$_8$-PIP$_2$. OT cells dialysed with diC$_8$-PIP$_2$ display slower rundown compared to controls over 30 min (Fig. 9B).

Changes in I_{mAHP} and I_{sAHP} via PIP$_2$ are unlikely to be the result of PLC-dependent phenomena

So far, we have demonstrated that a presumed reduction of PIP$_2$ by wortmannin caused a pronounced inhibition of the I_{mAHP} and I_{sAHP} in OT neurons, suggesting that PIP$_2$ is required for generation of both AHPs. While these results demonstrate the I_{mAHP} and I_{sAHP} require PIP$_2$, they do not provide any evidence for a mechanism by which PIP$_2$ can modulate I_{AHPs}. For example, PIP$_2$ could directly modulate the AHP channels. Alternatively, reduced PIP$_2$ levels could potentially act indirectly through PLC-induced inositol 1,4,5-trisphosphate (IP$_3$) or diacylglycerol (DAG) since PIP$_2$ is a precursor for breakdown by PLC into DAG and IP$_3$ (Suh & Hille, 2008). That is, blocking PIP$_2$ production by inhibiting the rate-limiting enzyme of production (PI4Kα) with wortmannin could cause a drop in PIP$_2$, which could in turn would reduce PLC-induced IP$_3$ availability (IP$_3$ binds to IP$_3$ receptors on the endoplasmic reticulum and induces Ca^{2+} release into the cytoplasm from internal stores: Dickson *et al.* 2013).

To test this, we used the selective PLC inhibitor U73122 (10 μM) to directly block the conversion of PIP$_2$ into DAG and IP$_3$ (Bleasdale *et al.* 1990; Pérez *et al.* 2010). U73122 has been widely used in the nervous system, including the
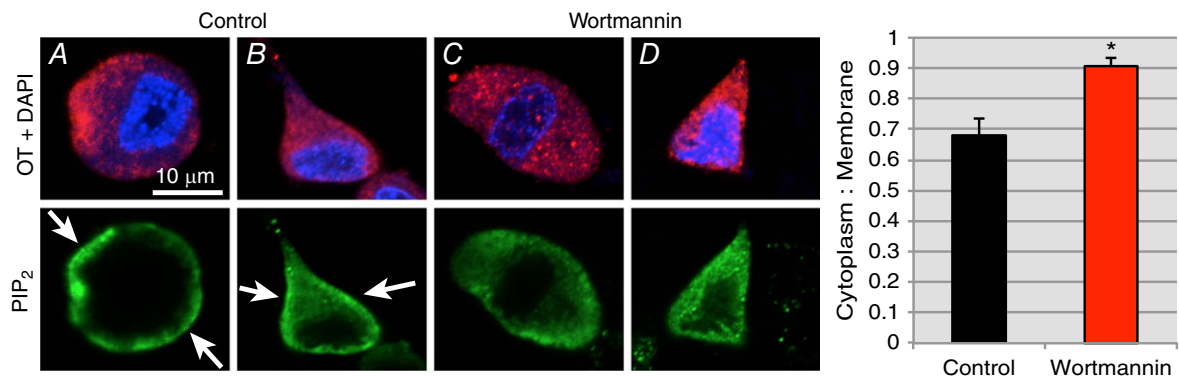

Figure 6. Effect of wortmannin on PIP$_2$ expression in OT neurons
Double immunofluorescence confocal microscopy revealed that PIP$_2$ (green) in OT neurons is expressed more densely in the cell membrane in the control group (*A* and *B*; lower panels). Upon wortmannin (100 nM) treatment for 30 min, OT neurons show a decreased PIP$_2$ expression in the cell membranes (*C* and *D*; lower panels) relative to the cytosol. The upper panels show the expression of OT-NP (red) expression and DAPI (blue) staining for nucleus. The histogram on the right side shows the mean cytoplasm: membrane ratios between the two groups, and indicates a significant difference (control *vs.* wortmannin; *$P \leq 0.016$). $n = 5$ animals per group.

study of PLC-dependent phenomena in SON (Sabatier *et al.* 1998; Li *et al.* 1999; Bonfardin *et al.* 2010). In OT neurons, U73122 had no effect on either the I_{mAHP} or the I_{sAHP} amplitude (100 ms: $n = 8$, $P > 0.05$; control 21.48 ± 2.4 pA *vs.* U73122 20.53 ± 3.1 pA; 1000 ms: $n = 8$, $P > 0.05$; control 3.45 ± 0.6 pA *vs.* U73122 3.42 ± 0.5 pA; Fig. 10). The decay time constant was also not significantly affected ($n = 8$, $P > 0.05$, control $\tau = 233.32 \pm 62.9$ ms *vs.* U73122 $\tau = 507.61 \pm 185.5$ ms; Fig. 10*B*). These results show it is unlikely that PIP$_2$ modulates the I_{AHP} by indirectly affecting downstream targets of PLC. This would primarily include Ca^{2+} release from stores via IP$_3$, or working through DAG and its product, protein kinase C (also known to modulate ion channels: Suh & Hille, 2008).

Changes in the I_{mAHP} and I_{sAHP} in OT neurons may be due to changes in Ca^{2+} influx

Unlike neocortical pyramidal cells where only the I_{sAHP} is affected by alterations in PIP$_2$ levels (Villalobos *et al.* 2011), all of our results in OT neurons occur in parallel for the I_{mAHP} and I_{sAHP}. A parsimonious explanation for this parallel effect is that PIP$_2$ exerts its effect upstream from the AHP K$^+$ channels on Ca^{2+} entry or Ca^{2+} availability. We hypothesized that PIP$_2$ may act on regulating Ca^{2+} entry or otherwise alter [Ca^{2+}]$_i$. To test this, we used Ca^{2+} imaging to determine whether wortmannin's inhibition of the AHPs in OT neurons affected [Ca^{2+}]$_i$. We used the high affinity Ca^{2+} indicator fura-2 (100 nM), as in our previous publications (Roper *et al.* 2003, 2004; Abel *et al.* 2004; Teruyama & Armstrong, 2005). The relative change in fura-2 fluorescence (%$\Delta F/F$) is linearly proportional to bulk [Ca^{2+}]$_i$ changes in the cytoplasm when %$\Delta F/F$ is less than ~0.5 (Abel *et al.* 2004). Since the peaks of bulk [Ca^{2+}]$_i$ were less than 0.5, we used the %$\Delta F/F$ value as an index for changes in [Ca^{2+}]$_i$. During the stimulus train,

we observed a rapid rise in [Ca^{2+}]$_i$ that decayed mono-exponentially (Fig. 11*C* and *D*). In OT neurons, we found that simultaneously with the reduction in I_{AHPs} (100 ms: $n = 9$, $P > 0.001$; control 30.23 ± 4.5 pA *vs.* wortmannin 9.77 ± 2.5 pA; 1000 ms: $P < 0.001$; control 7.64 ± 0.5 pA *vs.* wortmannin 4.09 ± 0.5 pA), wortmannin (1 μM) also reduced the spike-evoked increase in somatic [Ca^{2+}]$_i$ in OT neurons ($n = 9$, $P < 0.001$; control 44.09 ± 2.3 %$\Delta F/F$ *vs.* wortmannin 30.77 ± 2.4 %$\Delta F/F$; Fig. 11*A*, *C* and *E*). Consistent with our previous experiments showing no inhibition of AHPs, wortmannin had no effect on VP neuron I_{mAHPs} or I_{sAHPs} (100 ms: $n = 7$, $P > 0.05$; control 23.01 ± 4.6 pA *vs.* wortmannin 21.18 ± 3.98 pA; 1000 ms: $P > 0.05$; control 5.34 ± 1.1 pA *vs.* wortmannin 4.41 ± 0.9 pA; Fig. 11), or on [Ca^{2+}]$_i$ (control 47.40 ± 2.6 %$\Delta F/F$ *vs.* wortmannin 44.03 ± 2.9 %$\Delta F/F$;) (Fig. 11*B*, *D* and *E*).

PIP$_2$ depletion has no effect on AHPs generated by uncaging Ca^{2+}

The previous Ca^{2+} data suggest that PIP$_2$ modulates AHPs by changing Ca^{2+} entry or Ca^{2+} availability to the K$^+$ channels but does not rule out additional effects on the AHP channel itself. To test whether or not PIP$_2$ modulated AHP channels, we rapidly increased somatic [Ca^{2+}]$_i$ of the cell via photolytic release of Ca^{2+} from its caging compound, DM-nitrophen (2 mM). Neurons were dialysed with DM-nitrophen at 40% Ca^{2+} occupancy via the recording pipette and stimulated using a UV light flash from a xenon flash bulb. The result of this rapid Ca^{2+} release is an AHP generated without stimulating a train of action potentials in the cell, and thus an AHP independent of Ca^{2+} entry through voltage-gated Ca^{2+} ion channels (Sah & Clements, 1999). Using fluo-4 (50 μM) as the dye indicator for Ca^{2+}, we elicited AHPs with spiking and uncaging in every cell tested. We opted to
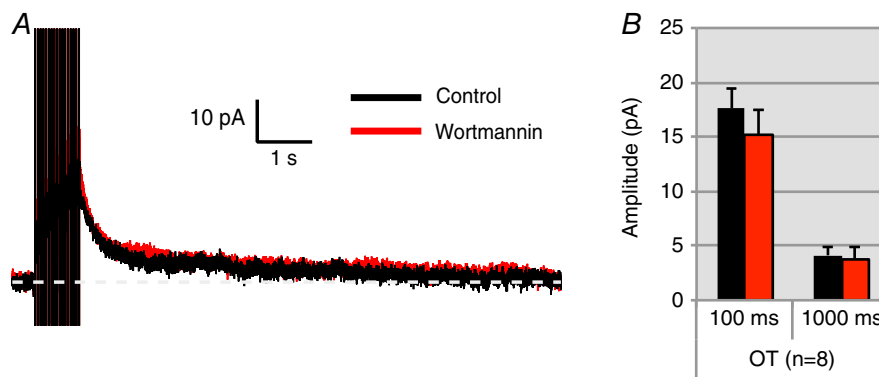

Figure 7. Dialysing OT neurons with diC$_8$-PIP$_2$ prevents inhibition of the I_{AHP} by wortmannin
A, I_{AHP} of an OT neuron dialysed with diC$_8$-PIP$_2$. diC$_8$-PIP$_2$ prevents inhibition of the I_{AHP} by wortmannin. *B*, summary data for 8 OT cells tested as in *A*. Measurements of the I_{AHP} 100 ms (I_{mAHP}) and 1000 ms (I_{sAHP}) after the pulse reveal that there are no significant changes in I_{AHP} peak amplitude after wortmannin application in diC$_8$-PIP$_2$ dialysed cells. (OT: $n = 8$, $P > 0.05$). [Colour figure can be viewed at wileyonlinelibrary.com]

use current clamp for these experiments for two reasons. (1) Signal fidelity was much better in current clamp. It was sometimes difficult to see an uncaged AHP in voltage clamp, while it was always clearly present in current clamp. (2) While still present in current clamp, rundown of both the currents and the Ca^{2+} transient was slower than the rundown we observed in voltage clamp.

For AHPs generated from current injections, we evoked action potentials with suprathreshold current using 20 10 ms pulses at 20 Hz, from a resting potential of ~ -55 mV (controlled by DC current injection). For AHPs generated from uncaging Ca^{2+}, we administered a UV light flash of ~ 1 ms duration at 72.6 J at the same membrane potential. To control for rundown, we measured AHPs at two time points for each of two groups: one control group and one group that received wortmannin application between the first and second measurements. Consistent with previous results in voltage clamp, both mAHPs and sAHPs generated by spiking were significantly inhibited by wortmannin application (100 ms: $n = 7$, $P < 0.001$; control 10.8 ± 0.6 mV *vs.* wortmannin 6.7 ± 1.2 mV; 1000 ms: $n = 7$, $P = 0.018$; control 8.3 ± 1.4 mV *vs.* wortmannin 4.6 ± 0.8 mV; Fig. 12*A*). The corresponding Ca^{2+} peak transients using fluo-4 were also inhibited significantly ($n = 7$, $P < 0.05$; control 45.2 ± 6.9 %$\Delta F/F$ *vs.* wortmannin 23.7 ± 4.1 %$\Delta F/F$; Fig. 12*B*). However, when AHPs were generated by uncaging Ca^{2+} in these same cells, we found no significant differences between groups in either the peak or 1000 ms uncaged AHP amplitude (peak: $P > 0.05$; control ($n = 7$) 10.0 ± 1.2 mV *vs.* wortmannin ($n = 8$) 13.9 ± 3.0 mV; 1000 ms: $P > 0.05$; control 7.9 ± 3.6 mV *vs.* wortmannin 10.5 ± 1.8 mV). Additionally, we found no change in the corresponding peak Ca^{2+} transient ($n = 7$, $P > 0.05$; control 128.6 ± 13.2 %$\Delta F/F$ *vs.* wortmannin 23.7 ± 4.1 %$\Delta F/F$; Fig. 12 *C* and *D*). This demonstrates that not only is PIP$_2$ likely

to modulate AHPs via spike-induced Ca^{2+} entry, but also that PIP$_2$ is not likely to gate the AHP channels themselves.

PIP$_2$ depletion inhibits whole cell Ca^{2+} currents in OT neurons

The results of our Ca^{2+} imaging and uncaging data suggest that PIP$_2$ affects the AHP by modulating Ca^{2+} entry through voltage-gated Ca^{2+} channels. To further test this, we isolated whole cell Ca^{2+} currents in slices using 0.0005 mM TTX, 50 mM TEA, and 5 mM CsCl, measured steady-state current responses to voltage steps, and plotted *I–V* curves before and after wortmannin application. Space clamp is a prevalent issue when measuring these currents in slice recordings of dendritic neurons, so cells exhibiting marked space clamp errors were excluded from analysis (criteria included delayed responses to voltage steps and escaping tail currents). Peak current occurred at a step to -10 mV, a result consistent with previous studies done on whole cell Ca^{2+} currents in these neurons (Fisher & Bourque, 1995; Foehring & Armstrong, 1996; Teruyama & Armstrong, 2005). Application of 400 μM Cd^{2+} after each trial resulted in a near complete block of current. When stepping positively, we started to observe inward current at the -40 mV step. At -10 mV where steady-state Ca^{2+} currents are largest, we observed a statistically significant inhibition by wortmannin ($n = 7$, $P = 0.018$; control -459.0 ± 41.1 pA *vs.* wortmannin -260.8 ± 23.9 pA; Fig. 13) in OT neurons. By comparison, VP neurons displayed no change in Ca^{2+} currents after application of wortmannin ($n = 5$, $P > 0.05$; control -482.5 $\pm$ 30.9 pA *vs.* wortmannin -493.8 ± 28.7 pA; Fig. 13). This result demonstrates PIP$_2$ modulates Ca^{2+} entry through voltage-gated Ca^{2+} channels.
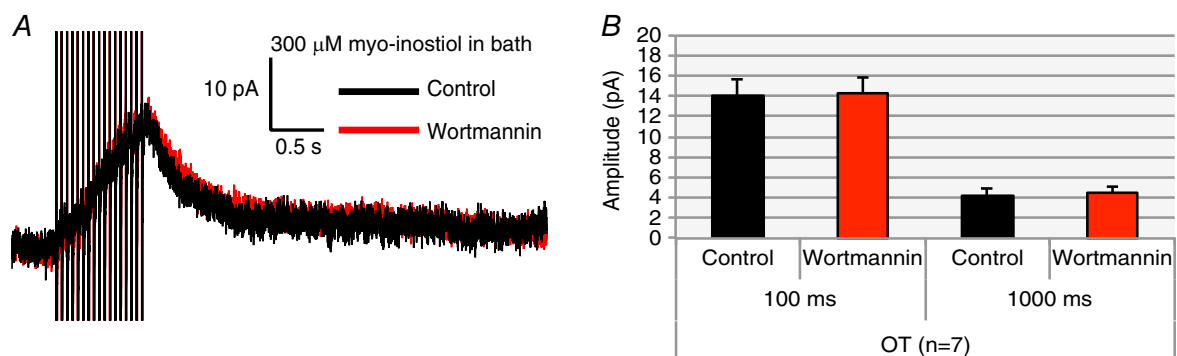

Figure 8. Wortmannin fails to inhibit OT neurons in aCSF containing myo-inositol
Slices were preincubated in aCSF containing 1 mM myo-inositol, an important precursor molecule for PIP$_2$ synthesis. When the slice was transported to the stage for patch clamp, the aCSF perfused onto the slice contained 300 μM myo-inositol during recording. *A*, voltage clamp trace of an OT neuron before and after application of wortmannin. Wortmannin had no effect on the OT *I*$_{AHP}$ when the cells were bathed in 300 μM myo-inositol. *B*, summary data for OT neurons. There were no significant differences in amplitude of current at 100 ms and 1000 ms after the pulse ($n = 7$, $P > 0.05$). [Colour figure can be viewed at wileyonlinelibrary.com]

Discussion

The AHP and its underlying currents are important regulators of intrinsic neuronal excitability. In SON neurons, they control the length and frequency of bursts of action potentials during phasic firing (Kirkpatrick & Bourque, 1996; Ghamari-Langroudi & Bourque, 2004). Despite the extensive work on the I_{sAHP}, the gating mechanism via Ca^{2+} is currently unknown. Furthermore, the mechanism appears to vary greatly depending on the neuronal cell type. In neocortical pyramidal cells, the unknown sAHP channels were found to track cytoplasmic $[Ca^{2+}]_i$ (Abel *et al.* 2004) and to be sensitive to PIP_2 manipulations (Villalobos *et al.* 2011). PIP_2 depletion by wortmannin reduced the I_{sAHP}, increasing PIP_2 levels by adding myo-inositol dramatically slowed I_{sAHP} rundown, and increasing PIP_2 by overexpression of PIP5K facilitated calcium activation of the I_{sAHP} (Villalobos *et al.* 2011). Together, these data suggest that in pyramidal neurons, PIP_2 may affect Ca^{2+} sensitivity of the I_{sAHP} channel.
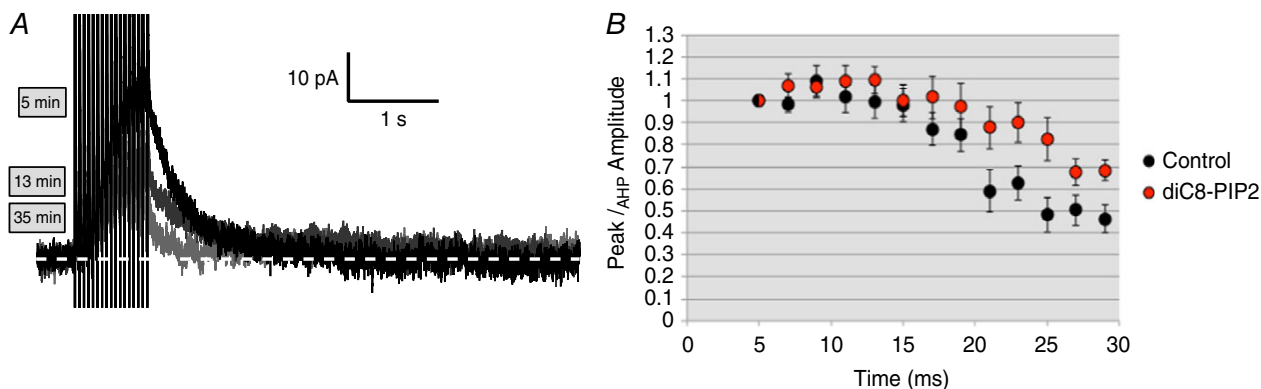

Figure 9. Inclusion of water-soluble PIP$_2$ analogue diC$_8$-PIP$_2$ (30 μm) in the recording pipette slows I_{AHP} rundown in OT

A, I_{AHP} recordings in an MNC under normal conditions demonstrating rundown over a 35 min time period. Both OT and VP cells display I_{AHP} rundown over long recording periods. *B*, OT cells dialysed with diC$_8$-PIP$_2$ display slower rundown and ran down less compared to controls at 30 min ($n = 9$). [Colour figure can be viewed at wileyonlinelibrary.com]
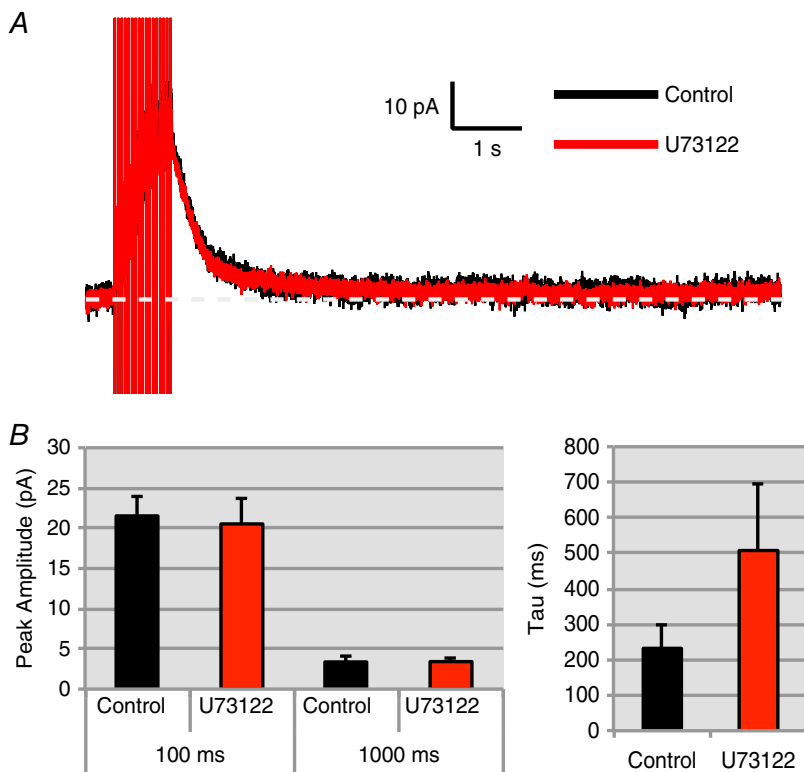

Figure 10. The PLC inhibitor U73122 (10 μm) failed to inhibit the I_{mAHP} or I_{sAHP} in OT neurons

A, voltage clamp trace of an OT neuron before and after application of U73122. *B*, summary data for OT neurons: current amplitude at 100 ms (I_{mAHP}), 1000 ms (I_{sAHP}), and I_{AHP} decay tau ($n = 8$, $P > 0.05$). [Colour figure can be viewed at wileyonlinelibrary.com]

Several K$^+$ channel types are known to require PIP$_2$ for activation, including KCNQ (K$_v$7) and K$_{ATP}$, among others (Hilgemann & Ball, 1996; Delmas & Brown, 2005 (p.7); Suh & Hille, 2008; Zaydman *et al.* 2013 (p.7); Eckey *et al.* 2014). In addition, the rundown during recordings of K$_v$7 and K$_{ATP}$ currents is a result of PIP$_2$ depletion (Hughes *et al.* 2007; Logothetis *et al.* 2007). Ca^{2+} channels also play a critical role in AHPs, as different channel species are coupled to the AHP depending on the cell type (Andrade *et al.* 2012). Many of these voltage-gated channels interact with PIP$_2$, and have been shown to have smaller currents when PIP$_2$ is depleted from the cells (Suh *et al.* 2010; Cruz *et al.* 2016). Because PIP$_2$ availability so greatly affected *I*$_{sAHP}$ generation in neocortical pyramidal cells, we tested the extent to which it could regulate the phenotypically similar *I*$_{AHPs}$ in SON.

Both OT and VP cells share core AHP features, including robust calcium dependence, voltage independence, modulation by neurotransmitters, and a relationship between amplitude and spike count (Alger & Nicoll, 1980; Lorenzon & Foehring, 1993; Ghamari-Langroudi & Bourque, 2004; Teruyama & Armstrong, 2005; Armstrong
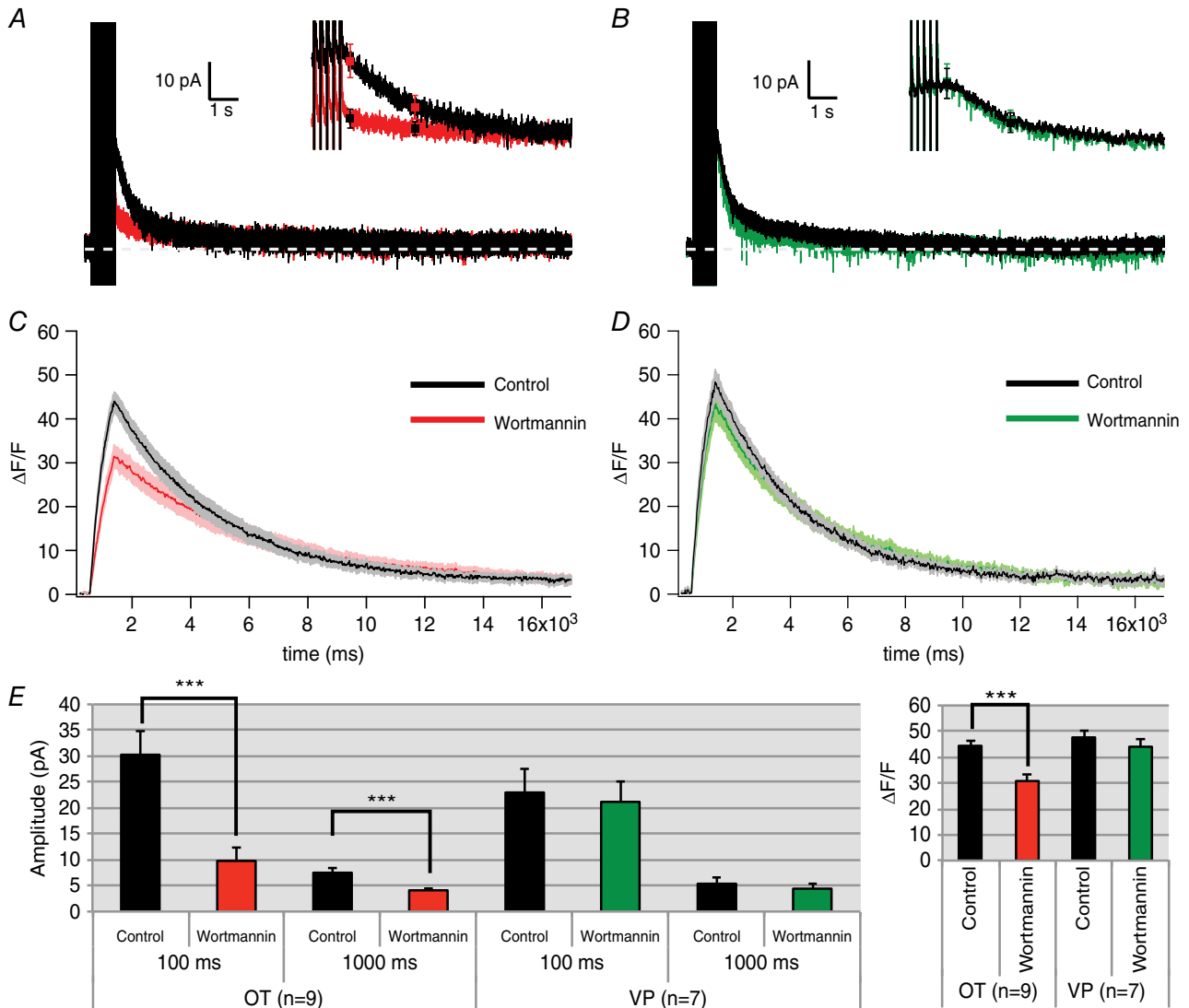

Figure 11. Wortmannin (1 μm) inhibits the *I*$_{mAHP}$, *I*$_{sAHP}$ and somatic Ca^{2+} while having no effect on these measures in VP neurons
A and *B*, averaged voltage clamp traces of OT (*A*) and VP (*B*) cells after wortmannin application; inset is higher temporal resolution of same trace with the mean ± SEM values superimposed at 100 ms and 1000 ms after the pulse. *C* and *D*, average intracellular Ca^{2+} response of OT (*C*) and VP (*D*) cells to wortmannin expressed as the change in fluorescence divided by the total fluorescence (%ΔF/F; shaded area of the curve is SEM). *E*, summary data at 100 ms (*I*$_{mAHP}$) and 1000 ms (*I*$_{sAHP}$) amplitude (OT: *n* = 9, 100 ms and 1000 ms ***P < 0.001; VP: *n* = 7, 100 ms and 500 ms *P* > 0.05) and summary data of Ca^{2+} transient peak amplitude (OT: *n* = 9, ***P < 0.001; VP: *n* = 7, *P* > 0.05). [Colour figure can be viewed at wileyonlinelibrary.com]
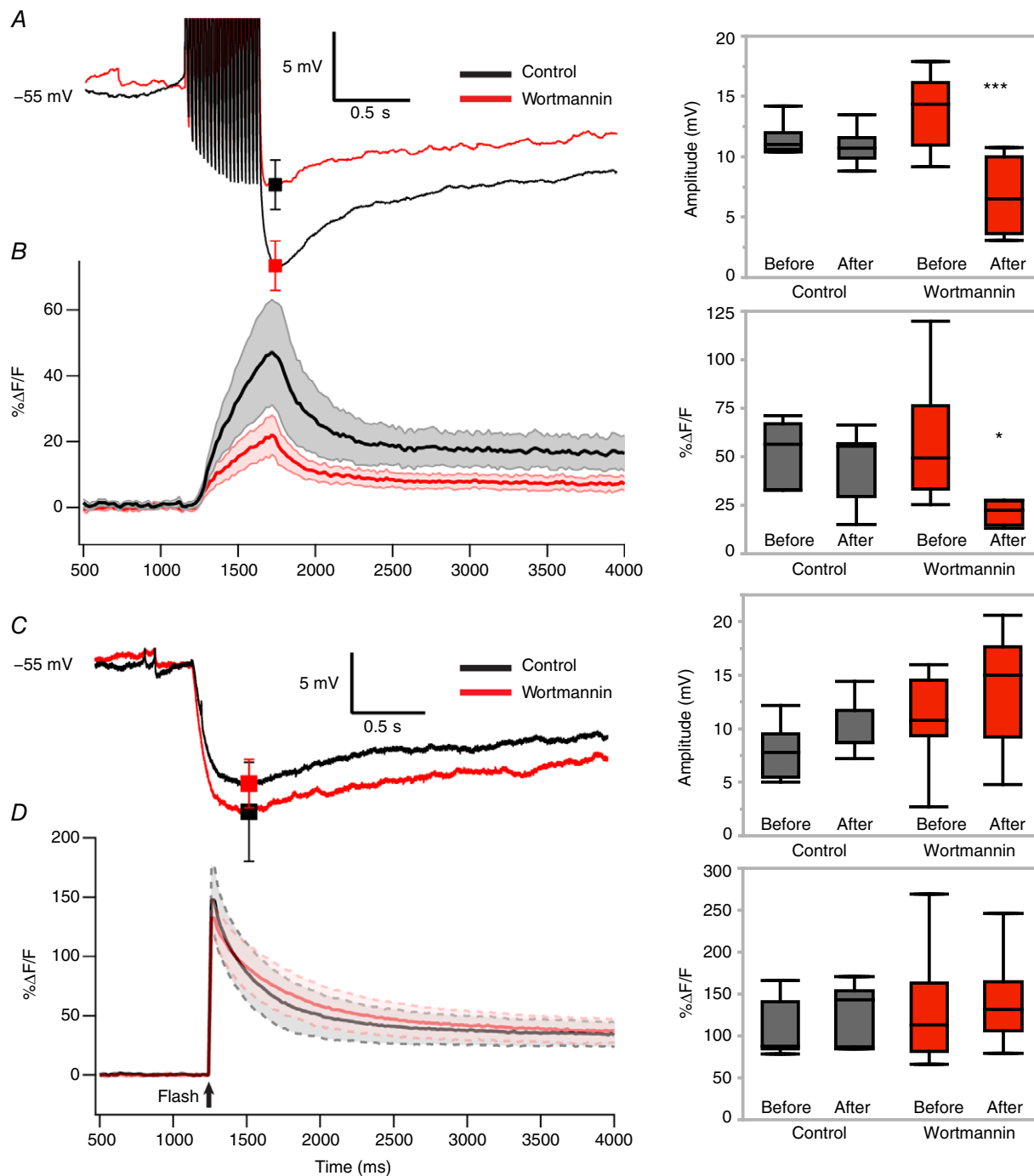
Figure 12. Wortmannin has no effect on AHPs or somatic Ca²⁺ when AHPs are generated via uncaging Ca²⁺ in OT neurons

Measurements of AHPs were taken at two time points to control for the rundown present in this experiment. In one group, wortmannin was administered between the two measurements. All example traces are group averages of the second measurement from the control and wortmannin groups. *A*, left, averaged current clamp traces of AHPs generated by trains of current injections with a superimposed mean $\pm$ SEM at 100 ms. *A*, right, box plot summary data of this effect (**$P = 0.008$). *B*, left, corresponding Ca²⁺ signal average for traces shown in *A*. Shaded area represents error. *B*, right, box plot summary data for Ca²⁺ transients generated by spike-generated AHPs (left) (*$P < 0.05$). *C*, left, averaged current clamp traces of AHPs generated by uncaging Ca²⁺ inside the cell with a superimposed mean $\pm$ SEM at the peak ($P > 0.05$). *C*, right, box plot summary data for uncaging-generated AHPs. *D*, left, corresponding Ca²⁺ signal average for traces shown in *C*. Shaded area represents error. *D*, right, box plot summary data for Ca²⁺ transients generated by an uncaging AHP ($P > 0.05$). [Colour figure can be viewed at wileyonlinelibrary.com]

et al. 2010; Andrade et al. 2012). Suggestions for the potassium channel underlying the sAHP channel across the nervous system include KCNQ, K$_{ATP}$, and IK channels. KCNQ channels have been an exceptional focus of study in this regard, considering the exhaustive documentation of their modulation by PIP$_2$ (Suh & Hille, 2002, 2007; Loussouarn et al. 2003; Li et al. 2005; Winks et al. 2005; Liu et al. 2008; Kim et al. 2016b). While KCNQ channels may be promising candidates for at least a component of the sAHP in some cells due to their modulation by PIP$_2$ (Loussouarn et al. 2003; Kim et al. 2016b), it is not clear whether a similar mechanism will hold for our results. For example, Kim et al. (2016b) revealed a complicated dynamic in CA1 pyramidal cells between the I_{sAHP}, the voltage dependence of KCNQ3 (K$_v$7.3) channels, and hippocalcin, a Ca^{2+} sensor protein critical for sAHP generation in CA1 neurons (Tzingounis et al.

2007). However, hippocalcin has not been found in the SON (Paterlini et al. 2000), and although KCNQ channels are expressed in the SON (Zhang et al. 2009b), and muscarinic suppression of sAHPs in SON has been reported, the sAHP does not show any voltage dependence (Ghamari-Langroudi & Bourque, 2004), some of which would be expected if underlain by KCNQ channels. The latter authors did rule out BK, SK, and IK channels, however, based on the insensitivity of the sAHP to toxins targeting these toxins (Ghamari-Langroudi & Bourque, 2004).

In SON neurons, we demonstrate an observable mechanistic difference between two similar cell types in the same nucleus. Depletion of PIP$_2$ inhibits both the medium and slow components of the AHP in OT neurons while having no discernable effect on VP neurons. This is a novel and perhaps surprising result.
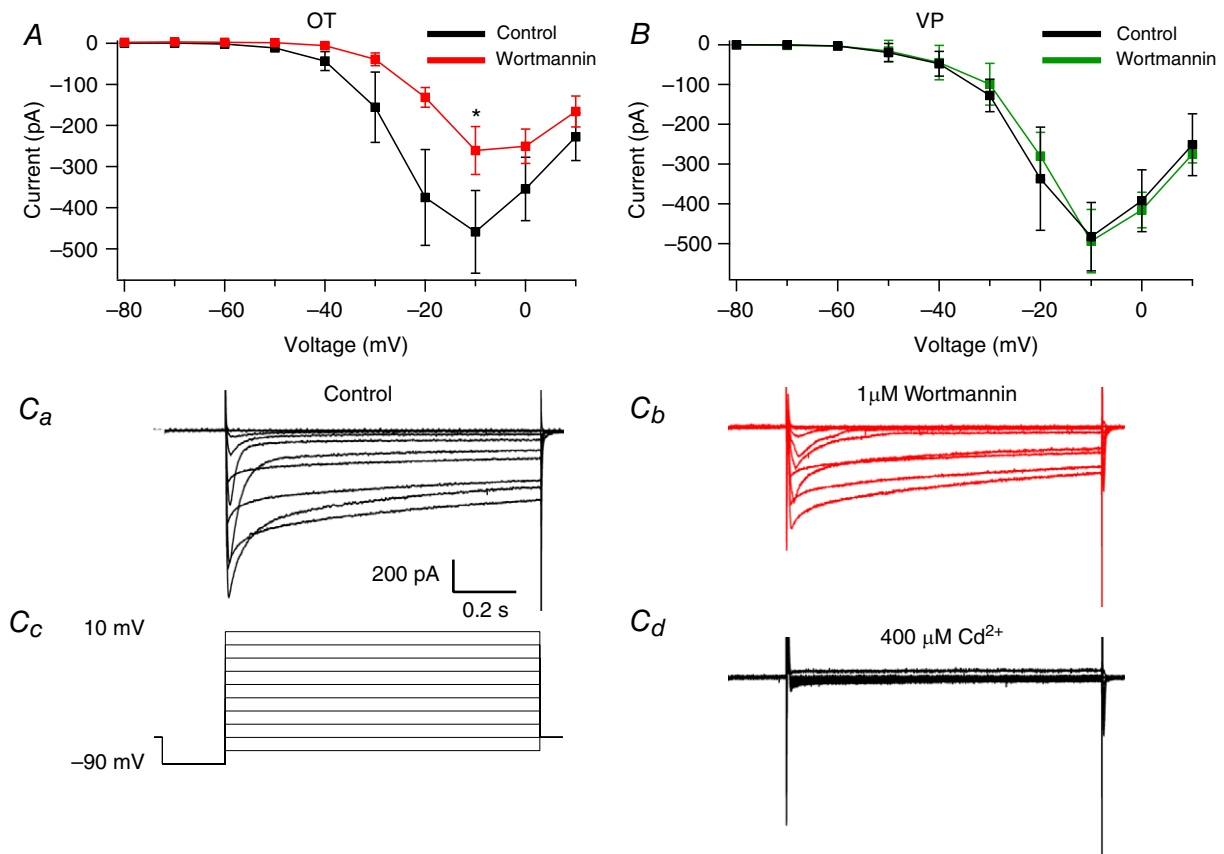

Figure 13. Wortmannin inhibits whole cell Ca^{2+} currents in OT neurons while having no effect in VP neurons
Ca^{2+} currents were isolated and subsequently measured before and after wortmannin (1 μM). I–V curves were plotted from steady-state measurements of these currents. A, I–V curve of Ca^{2+} currents before and after wortmannin in OT neurons. Comparison at the highest amplitude steady-state current (−10 mV) revealed a significant difference (*P < 0.05). B, I–V curve of Ca^{2+} currents before and after wortmannin in VP neurons. C, example traces from a single OT neuron of isolated whole cell Ca^{2+} currents generated by voltage steps from −90 mV to +10 mV under control conditions (Ca) and after 1 μM wortmannin application (Cb). The voltage protocol (Cc) and 400 μM Cd^{2+} (Cd) are shown for the same cell. [Colour figure can be viewed at wileyonlinelibrary.com]

Previous studies described cell type differences in firing patterns and plasticity during the reproductive cycle, but this is the first description of an OT–VP difference in an AHP mechanism (Bourque *et al.* 1985; Armstrong, 1995; Teruyama & Armstrong, 2002, 2005). Perhaps the differences are related to the fact that AHP and spike frequency undergo massive plastic changes in OT neurons during pregnancy and lactation, while VP neurons remain mostly unaffected in this regard. Thus PIP$_2$ activity could be a key regulator of AHP changes during the reproductive cycle.

Differences between our results in SON and previous results in neocortical neurons are twofold. First, PIP$_2$ depletion blocked both the I_{mAHP} and I_{sAHP} in OT neurons (with no effect in VP neurons), whereas it only affected the I_{sAHP} in neocortical neurons (Villalobos *et al.* 2011). This is demonstrated by wortmannin block at 100 ms (mAHP) and 1000 ms (sAHP) after the stimulus (Fig. 3) and inhibition of isolated I_{sAHP} currents in the presence of apamin (Fig. 5). Second, $[Ca^{2+}]_i$ transients are reduced after PIP$_2$ depletion in OT neurons (Fig. 11) whereas neocortical $[Ca^{2+}]_i$ transients were unaffected by PIP$_2$ depletion. These differences reflect a novel distinction between AHP mechanisms of different cell types. The results in cortex are likely to reflect a change in Ca^{2+} sensitivity of the AHP while the results in OT neurons appear to reflect a change in Ca^{2+} entry through voltage-gated Ca^{2+} channels.

Wortmannin-induced inhibition of I_{AHPs} results from a restriction of PIP$_2$ availability

Wortmannin consistently and effectively blocked the I_{mAHP} and I_{sAHP} in OT neurons in a dose-dependent manner (Figs 3 and 11). Because wortmannin has multiple targets and drastic effects on OT AHPs, careful dissection of its effects was carried out in this study. One potential confound is non-specific effects of wortmannin, since this drug inhibits more than PI4Kα. In fact, wortmannin is an inhibitor of PI3K activity as well as the PI3K–Akt signal transduction pathway (Nakanishi *et al.* 1995; Brunn *et al.* 1996). PI3K is actually the higher affinity target of wortmannin (IC$_{50}$ = 2–4 nM), as opposed to its effect on PI4Kα (IC$_{50}$ ≈ 50 nM) (Nakanishi *et al.* 1995). The previously reported IC$_{50}$ for wortmannin's effect on PI4Kα is consistent with our dose–response curve generated by the proportion of peak I_{AHP} inhibition (IC$_{50}$ = 58 nM), which was well fitted by a single Langmuir isotherm with a Hill coefficient of 1.6. Consistent with the IC$_{50}$ matching PI4Kα inhibition, the more specific PI3K inhibitor LY294,002 failed to affect the I_{mAHP} and I_{sAHP} in OT neurons (Fig. 4). Elevating PIP$_2$ levels by supplementing the internal solution with diC$_8$-PIP$_2$ (Fig. 7), or by exposing the cells to myo-inositol (Fig. 8), prevented I_{mAHP} and I_{sAHP} inhibition by wortmannin. We also demonstrated that wortmanin increases the cytoplasm:membrane ratio of PIP$_2$ in dissociated OT neurons (Fig. 6). This result has also been reported with oxotremorine-M in MNCs with immunochemistry (Shah *et al.* 2014), and is consistent with a study in which wortmannin prevented the recovery of M-currents after PIP$_2$ depletion via oxotremorine-M, confirming its inhibitory activity on PIP$_2$ synthesis (Suh & Hille, 2002). Together, these results demonstrate that wortmannin blocks the I_{AHP} by inhibiting PIP$_2$ production and that PIP$_2$ availability is critical for generation of the I_{mAHP} and I_{sAHP} in OT neurons. The robust inhibition of both medium and slow components suggests PIP$_2$ affects a common mechanism between the two. The most recognizable connection is the Ca^{2+} dependence of the I_{mAHP} and I_{sAHP}.

PIP$_2$ depletion alters Ca^{2+} entry through voltage-gated Ca^{2+} channels in OT neurons

We hypothesized that PIP$_2$ affected either Ca^{2+} entry or Ca^{2+} availability to the AHP channels. We first considered that depleting PIP$_2$ was effectively limiting Ca^{2+} release from IP$_3$-gated Ca^{2+} stores, shown to be a source of AHP-related Ca^{2+} in dopamine neurons (Morikawa *et al.* 2000). To the extent that U73122 is specific to PLC inhibition, this application had no effect on the I_{mAHP} or I_{sAHP} of OT neurons (Fig. 10), consistent with the hypothesis that downstream targets of PLC activity are not involved. In contrast, both Ca^{2+} transients and whole cell Ca^{2+} currents were suppressed by wortmannin in OT, but not VP neurons, suggesting that PIP$_2$ is interacting with voltage-gated Ca^{2+} channels in these cells. This conclusion was further strengthened by a lack of wortmannin's effect on uncaging-invoked AHPs (Fig. 12). Thus, PIP$_2$ depletion simultaneously inhibits AHPs, Ca^{2+} transients, and Ca^{2+} currents in OT neurons. Though this result contrasts with observations in cortical neurons, the data do not necessarily rule out Ca^{2+} sensitivity as contributing to the effect on the I_{sAHP}.

Although we observed clear inhibition of HVA currents with wortmannin, several voltage-activated Ca^{2+} channels are candidates for the PIP$_2$ modulation. It is presently unknown which specific Ca^{2+} channel types couple to the medium and slow AHP in OT and VP neurons in the SON. MNCs express high-voltage-activated (HVA) L-, N-, P/Q-type, and R type channels, as demonstrated with mRNA (Glasgow *et al.* 1999), immunochemistry (Joux *et al.* 2001) and pharmacological block of whole cell currents in voltage clamp (Fisher & Bourque, 1995; Foehring & Armstrong, 1996), although these studies did not differentiate between OT and VP neurons. Importantly, HVAs have been demonstrated to interact with PIP$_2$ (Suh *et al.* 2010; Kim *et al.* 2016a; Cruz *et al.* 2016). Transient, low-threshold-activated (LVA) type Ca^{2+} channels may also contribute to AHPs, and

these have been reported in MNCs by some (Erickson *et al.* 1993; Fisher & Bourque, 1995; Israel *et al.* 2008), although not by all investigators (Foehring & Armstrong, 1996; Luther & Tasker, 2000; Joux *et al.* 2001; Luther *et al.* 2002). Nevertheless, LVAs clearly contribute to sAHPs in thalamic paraventricular neurons (Zhang *et al.* 2009*a*). Channel coupling may also be different for the mAHP and sAHP. Previous work describes mAHPs being activated by restricted microdomains of membrane Ca^{2+}, while the sAHP has a tighter, cooperative sigmoidal relationship with bulk somatic [Ca^{2+}]$_i$ (Wilson & Callaway, 2000; Abel *et al.* 2004). Therefore, the sAHP inhibition caused by PIP$_2$ depletion could be caused by an inhibition of multiple Ca^{2+} channel species providing diffusible Ca^{2+}. Interestingly, N-type channels contribute to peptide release in OT and VP neurons, while P/Q channels contribute only in VP neurons in this regard (Wang & Fisher, 2014). This trait might provide a clue about cell-type differences for PIP$_2$ modulation of HVA channels.

It is important to explicitly mention that our results do not assume the same mechanisms for both the I_{mAHP} and I_{sAHP}, just that PIP$_2$ is a regulator of both, and both are dependent on modulation of Ca^{2+} entry. For example, previous work demonstrated that PIP$_2$ is a necessary cofactor for SK channel activation, binding to the CaM–SK interface on these channels to shift Ca$^+$ sensitivity (Zhang *et al.* 2014). Though this work was done on SK2 channels, the SK3 channel complex also contains CaM, and its modulation in this manner remains a possibility for gating the I_{mAHP} in SON.

References

Abel HJ, Lee JCF, Callaway JC & Foehring RC (2004). Relationships between intracellular calcium and afterhyperpolarizations in neocortical pyramidal neurons. *J Neurophysiol* **91**, 324–335.

Alger BE & Nicoll RA (1980). Epileptiform burst afterhyperpolarization: calcium-dependent potassium potential in hippocampal CA1 pyramidal cells. *Science* **210**, 1122–1124.

Andrade R, Foehring RC & Tzingounis AV (2012). The calcium-activated slow AHP: cutting through the Gordian knot. *Front Cell Neurosci* **6**, 47.

Armstrong WE (1995). Morphological and electrophysiological classification of hypothalamic supraoptic neurons. *Prog Neurobiol* **47**, 291–339.

Armstrong WE, Smith BN & Tian M (1994). Electrophysiological characteristics of immunochemically identified rat oxytocin and vasopressin neurones *in vitro*. *J Physiol* **475**, 115–128.

Armstrong WE, Wang L., Li C & Teruyama R (2010). Performance, properties and plasticity of identified oxytocin and vasopressin neurones *in vitro*. *J Neuroendocrinol* **22**, 330–342.

Belin V, Moos F & Richard P (1984). Synchronization of oxytocin cells in the hypothalamic paraventricular and supraoptic nuclei in suckled rats: direct proof with paired extracellular recordings. *Exp Brain Res* **57**, 201–203.

Bicknell RJ (1988). Optimizing release from peptide hormone secretory nerve terminals. *J Exp Biol* **139**, 51–65.

Bicknell RJ & Leng G (1981). Relative efficiency of neural firing patterns for vasopressin release *in vitro*. *Neuroendocrinology* **33**, 295–299.

Bleasdale JE, Thakur NR, Gremban RS, Bundy GL, Fitzpatrick FA, Smith RJ & Bunting S (1990). Selective inhibition of receptor-coupled phospholipase C-dependent processes in human platelets and polymorphonuclear neutrophils. *J Pharmacol Exp Ther* **255**, 756–768.

Bonfardin VDJ, Fossat P, Theodosis DT & Oliet SHR (2010). Glia-dependent switch of kainate receptor presynaptic action. *J Neurosci* **30**, 985–995.

Bourque CW & Brown DA (1987). Apamin and d-tubocurarine block the after-hyperpolarization of rat supraoptic neurosecretory neurons. *Neurosci Lett* **82**, 185–190.

Bourque CW, Randle JC & Renaud LP (1985). Calcium-dependent potassium conductance in rat supraoptic nucleus neurosecretory neurons. *J Neurophysiol* **54**, 1375–1382.

Brunn GJ, Williams J, Sabers C, Wiederrecht G, Lawrence JC & Abraham RT (1996). Direct inhibition of the signaling functions of the mammalian target of rapamycin by the phosphoinositide 3-kinase inhibitors, wortmannin and LY294002. *EMBO J* **15**, 5256–5267.

Cazalis M, Dayanithi G & Nordmann JJ (1985). The role of patterned burst and interburst interval on the excitation-coupling mechanism in the isolated rat neural lobe. *J Physiol* **369**, 45–60.

Cruz L de la, Puente EI, Reyes-Vaca A, Arenas I, Garduño J, Bravo-Martínez J & Garcia DE (2016). PIP$_2$ in pancreatic *β*-cells regulates voltage-gated calcium channels by a voltage-independent pathway. *Am J Physiol Cell Physiol* **311**, C630–C640.

Delmas P & Brown DA (2005). Pathways modulating neural KCNQ/M (Kv7) potassium channels. *Nat Rev Neurosci* **6**, 850–862.

Dickson EJ, Falkenburger BH & Hille B (2013). Quantitative properties and receptor reserve of the IP$_3$ and calcium branch of Gq-coupled receptor signaling. *J Gen Physiol* **141**, 521–535.

Dopico AM, Widmer H, Wang G, Lemos JR & Treistman SN (1999). Rat supraoptic magnocellular neurones show distinct large conductance, Ca^{2+}-activated K$^+$ channel subtypes in cell bodies *versus* nerve endings. *J Physiol* **519**, 101–114.

Drummond GB (2009). Reporting ethical matters in The Journal of Physiology: standards and advice. *J Physiol* **587**, 713–719.

Dutton A & Dyball REJ (1979). Phasic firing enhances vasopressin release from the rat neurohypophysis. *J Physiol* **290**, 433–440.

Eckey K, Wrobel E, Strutz-Seebohm N, Pott L, Schmitt N & Seebohm G (2014). Novel Kv7.1-phosphatidylinositol 4,5-bisphosphate interaction sites uncovered by charge neutralization scanning. *J Biol Chem* **289**, 22749–22758.

Erickson KR, Ronnekleiv OK & Kelly MJ (1993). Role of a T-type calcium current in supporting a depolarizing potential, damped oscillations, and phasic firing in vasopressinergic guinea pig supraoptic neurons. *Neuroendocrinology* **57**, 789–800.

Fisher SK, Heacock AM & Agranoff BW (1992). Inositol lipids and signal transduction in the nervous system: an update. *J Neurochem* **58**, 18–38.

Fisher SK, Novak JE & Agranoff BW (2002). Inositol and higher inositol phosphates in neural tissues: homeostasis, metabolism and functional significance. *J Neurochem* **82**, 736–754.

Fisher TE & Bourque CW (1995). Voltage-gated calcium currents in the magnocellular neurosecretory cells of the rat supraoptic nucleus. *J Physiol* **486**, 571–580.

Foehring RC & Armstrong WE (1996). Pharmacological dissection of high-voltage-activated Ca^{2+} current types in acutely dissociated rat supraoptic magnocellular neurons. *J Neurophysiol* **76**, 977–983.

Ghamari-Langroudi M & Bourque CW (1998). Caesium blocks depolarizing after-potentials and phasic firing in rat supraoptic neurones. *J Physiol* **510**, 165–175.

Ghamari-Langroudi M & Bourque C (2004). Muscarinic receptor modulation of slow afterhyperpolarization and phasic firing in rat supraoptic nucleus neurons. *J Neurosci* **24**, 7718–7726.

Glasgow E, Kusano K, Chin H, Mezey E, Young WS & Gainer H (1999). Single cell reverse transcription-polymerase chain reaction analysis of rat supraoptic magnocellular neurons: neuropeptide phenotypes and high voltage-gated calcium channel subtypes. *Endocrinology* **140**, 5391–5401.

Grundy D (2015). Principles and standards for reporting animal experiments in *The Journal of Physiology* and *Experimental Physiology*. *J Physiol* **593**, 2547–2549.

Higuchi T, Uchide K, Honda K & Negoro H (1986). Oxytocin release during parturition in the pelvic-neurectomized rat. *J Endocrinol* **109**, 149–154.

Hilgemann DW & Ball R (1996). Regulation of cardiac Na^+,Ca^{2+} exchange and K_{ATP} potassium channels by PIP_2. *Science* **273**, 956–959.

Hille B (1994). Modulation of ion-channel function by G-protein-coupled receptors. *Trends Neurosci* **17**, 531–536.

Hlubek MD & Cobbett P (2000). Differential effects of K^+ channel blockers on frequency-dependent action potential broadening in supraoptic neurons. *Brain Res Bull* **53**, 203–209.

Hughes S, Marsh SJ, Tinker A & Brown DA (2007). PIP_2-dependent inhibition of M-type (Kv7.2/7.3) potassium channels: direct on-line assessment of PIP_2 depletion by Gq-coupled receptors in single living neurons. *Pflügers Archiv* **455**, 115–124.

Israel J-M, Poulain DA & Oliet SHR (2008). Oxytocin-induced postinhibitory rebound firing facilitates bursting activity in oxytocin neurons. *J Neurosci* **28**, 385–394.

Joux N, Chevaleyre V, Alonso G, Boissin-Agasse L, Moos FC, Desarménien MG & Hussy N (2001). High voltage-activated Ca^{2+} currents in rat supraoptic neurones: biophysical properties and expression of the various channel alpha1 subunits. *J Neuroendocrinol* **13**, 638–649.

Kim D-I, Kweon H-J, Park Y, Jang D-J & Suh B-C (2016*a*). Ca^{2+} controls gating of voltage-gated calcium channels by releasing the β2e subunit from the plasma membrane. *Sci Signal* **9**, ra67-ra67.

Kim KS, Duignan KM, Hawryluk JM, Soh H & Tzingounis AV (2016*b*). The voltage activation of cortical KCNQ channels depends on global PIP_2 levels. *Biophys J* **110**, 1089–1098.

Kirkpatrick K & Bourque CW (1996). Activity dependence and functional role of the apamin-sensitive K^+ current in rat supraoptic neurones *in vitro*. *J Physiol* **494**, 389–398.

Kruse M & Hille B (2013). The phosphoinositide sensitivity of the KV channel family. *Channels* **7**, 530–536.

Lasser-Ross N, Miyakawa H, Lev-Ram V, Young SR & Ross WN (1991). High time resolution fluorescence imaging with a CCD camera. *J Neurosci Methods* **36**, 253–261.

Lee J, Jung K, Kim YS & Park D (2007). Diosgenin inhibits melanogenesis through the activation of phosphatidylinositol-3-kinase pathway (PI3K) signaling. *Life Sci* **81**, 249–254.

Li Y, Gamper N, Hilgemann DW & Shapiro MS (2005). Regulation of Kv7 (KCNQ) K^+ channel open probability by phosphatidylinositol 4,5-bisphosphate. *J Neurosci* **25**, 9825–9835.

Li Z, Miyata S & Hatton GI (1999). Inositol 1,4,5-trisphosphate-sensitive Ca^{2+} stores in rat supraoptic neurons: involvement in histamine-induced enhancement of depolarizing afterpotentials. *Neuroscience* **93**, 667–674.

Liu B, Liang H, Liu L & Zhang H (2008). Phosphatidylinositol 4,5-bisphosphate hydrolysis mediates histamine-induced KCNQ/M current inhibition. *Am J Physiol Cell Physiol* **295**, C81–C91.

Logothetis DE, Jin T, Lupyan D & Rosenhouse-Dantsker A (2007). Phosphoinositide-mediated gating of inwardly rectifying K^+. *Pflügers Archiv* **455**, 83–95.

Lorenzon NM & Foehring RC (1993). The ontogeny of repetitive firing and its modulation by norepinephrine in rat neocortical neurons. *Brain Res Dev Brain Res* **73**, 213–223.

Loussouarn G, Park K-H, Bellocq C, Baró I, Charpentier F & Escande D (2003). Phosphatidylinositol-4,5-bisphosphate, PIP_2, controls KCNQ1/KCNE1 voltage-gated potassium channels: a functional homology between voltage-gated and inward rectifier K^+ channels. *EMBO J* **22**, 5412–5421.

Luther JA, Daftary SS, Boudaba C, Gould GC, Halmos KC & Tasker JG (2002). Neurosecretory and non-neurosecretory parvocellular neurones of the hypothalamic paraventricular nucleus express distinct electrophysiological properties. *J Neuroendocrinol* **14**, 929–932.

Luther JA & Tasker JG (2000). Voltage-gated currents distinguish parvocellular from magnocellular neurones in the rat hypothalamic paraventricular nucleus. *J Physiol* **523**, 193–209.

Meyers R & Cantley LC (1997). Cloning and characterization of a wortmannin-sensitive human phosphatidylinositol 4-kinase. *J Biol Chem* **272**, 4384–4390.

Morikawa H, Imani F, Khodakhah K & Williams JT (2000). Inositol 1,4,5-triphosphate-evoked responses in midbrain dopamine neurons. *J Neurosci* **20**, RC103.

Nakanishi S, Catt KJ & Balla T (1995). A wortmannin-sensitive phosphatidylinositol 4-kinase that regulates hormone-sensitive pools of inositolphospholipids. *Proc Natl Acad Sci USA* **92**, 5317–5321.

Paterlini M, Revilla V, Grant AL & Wisden W (2000). Expression of the neuronal calcium sensor protein family in the rat brain. *Neuroscience* **99**, 205–216.

Pérez C, Vega R & Soto E (2010). Phospholipase C-mediated inhibition of the M-potassium current by muscarinic-receptor activation in the vestibular primary-afferent neurons of the rat. *Neurosci Lett* **468**, 238–242.

Poulain DA & Wakerley JB (1982). Electrophysiology of hypothalamic magnocellular neurones secreting oxytocin and vasopressin. *Neuroscience* **7**, 773–808.

Roper P, Callaway J & Armstrong W (2004). Burst initiation and termination in phasic vasopressin cells of the rat supraoptic nucleus: a combined mathematical, electrical, and calcium fluorescence study. *J Neurosci* **24**, 4818–4831.

Roper P, Callaway J, Shevchenko T, Teruyama R & Armstrong W (2003). AHP's, HAP's and DAP's: how potassium currents regulate the excitability of rat supraoptic neurones. *J Comput Neurosci* **15**, 367–389.

Sabatier N & Leng G (2007). Bistability with hysteresis in the activity of vasopressin cells. *J Neuroendocrinol* **19**, 95–101.

Sabatier N, Richard P & Dayanithi G (1998). Activation of multiple intracellular transduction signals by vasopressin in vasopressin-sensitive neurones of the rat supraoptic nucleus. *J Physiol* **513**, 699–710.

Sah P & Clements JD (1999). Photolytic manipulation of $[Ca^{2+}]_i$ reveals slow kinetics of potassium channels underlying the afterhyperpolarization in hipppocampal pyramidal neurons. *J Neurosci* **19**, 3657–3664.

Shah L, Bansal V, Rye PL, Mumtaz N, Taherian A & Fisher TE (2014). Osmotic activation of phospholipase C triggers structural adaptation in osmosensitive rat supraoptic neurons. *J Physiol* **592**, 4165–4175.

Stern JE & Armstrong WE (1996). Changes in the electrical properties of supraoptic nucleus oxytocin and vasopressin neurons during lactation. *J Neurosci* **16**, 4861–4871.

Stocker M & Pedarzani P (2000). Differential distribution of three Ca^{2+}-activated K^+ channel subunits, SK1, SK2, and SK3, in the adult rat central nervous system. *Mol Cell Neurosci* **15**, 476–493.

Suh B-C & Hille B (2002). Recovery from muscarinic modulation of M current channels requires phosphatidylinositol 4,5-bisphosphate synthesis. *Neuron* **35**, 507–520.

Suh B-C & Hille B (2007). Electrostatic interaction of internal Mg^{2+} with membrane PIP$_2$ seen with KCNQ K$^+$ channels. *J Gen Physiol* **130**, 241–256.

Suh B-C & Hille B (2008). PIP$_2$ is a necessary cofactor for ion channel function: how and why? *Annu Rev Biophys* **37**, 175–195.

Suh B-C, Leal K & Hille B (2010). Modulation of high-voltage activated Ca^{2+} channels by membrane phosphatidylinositol 4,5-bisphosphate. *Neuron* **67**, 224–238.

Tacconi S, Carletti R, Bunnemann B, Plumpton C, Merlo Pich E & Terstappen GC (2001). Distribution of the messenger RNA for the small conductance calcium-activated potassium channel SK3 in the adult rat brain and correlation with immunoreactivity. *Neuroscience* **102**, 209–215.

Teruyama R & Armstrong WE (2002). Changes in the active membrane properties of rat supraoptic neurones during pregnancy and lactation. *J Neuroendocrinol* **14**, 933–944.

Teruyama R & Armstrong WE (2005). Enhancement of calcium-dependent afterpotentials in oxytocin neurons of the rat supraoptic nucleus during lactation. *J Physiol* **566**, 505–518.

Teruyama R & Armstrong WE (2007). Calcium-dependent fast depolarizing afterpotentials in vasopressin neurons in the rat supraoptic nucleus. *J Neurophysiol* **98**, 2612–2621.

Tzingounis AV, Kobayashi M, Takamatsu K & Nicoll RA (2007). The diffusible calcium sensor, hippocalcin, gates the calcium activation of the slow afterhyperpolarization in hippocampal pyramidal neurons. *Neuron* **53**, 487–493.

Vanhaesebroeck, B, Leevers SJ, Ahmadi K, Timms J, Katso R, Driscoll PC, Woscholski R, Parker PJ & Waterfield MD (2001). Synthesis and function of 3-phosphorylated inositol lipids. *Annu Rev Biochem* **70**, 535–602.

Villalobos C, Foehring RC, Lee JC & Andrade R (2011). Essential role for phosphatidylinositol 4,5-bisphosphate in the expression, regulation, and gating of the slow afterhyperpolarization current in the cerebral cortex. *J Neurosci* **31**, 18303–18312.

Vlahos CJ, Matter WF, Hui KY & Brown RF (1994). A specific inhibitor of phosphatidylinositol 3-kinase, 2-(4-morpholinyl)-8-phenyl-4H-1-benzopyran-4-one (LY294002). *J Biol Chem* **269**, 5241–5248.

Wakerly JB & Lincoln DW (1971). Milk ejection in the rat: recordings of intramammary pressure during suckling. *J Endocrinol* **51**, 13–14.

Wang D & Fisher TE (2014). Expression of CaV 2.2 and splice variants of CaV 2.1 in oxytocin- and vasopressin-releasing supraoptic neurones. *J Neuroendocrinol* **26**, 100–110.

Wang Q, Xia X, Deng X, Li N, Wu D, Zhang L, Yang C, Tao F & Zhou J (2016). Lambda-cyhalothrin disrupts the up-regulation effect of 17β-estradiol on post-synaptic density 95 protein expression via estrogen receptor α-dependent Akt pathway. *J Environ Sci China* **41**, 252–260.

Wilson CJ & Callaway JC (2000). Coupled oscillator model of the dopaminergic neuron of the substantia nigra. *J Neurophysiol* **83**, 3084–3100.

Winks JS, Hughes S, Filippov AK, Tatulian L, Abogadie FC, Brown DA & Marsh SJ (2005). Relationship between membrane phosphatidylinositol-4,5-bisphosphate and receptor-mediated inhibition of native neuronal M channels. *J Neurosci* **25**, 3400–3413.

Zaydman MA, Silva JR, Delaloye K, Li Y, Liang H, Larsson HP, Shi J & Cui J (2013). Kv7.1 ion channels require a lipid to couple voltage sensing to pore opening. *Proc Natl Acad Sci USA* **110**, 13180–13185.

Zhang L, Renaud LP & Kolaj M (2009*a*). Properties of a T-Type Ca^{2+} channel-activated slow afterhyperpolarization in thalamic paraventricular nucleus and other thalamic midline neurons. *J Neurophysiol* **101**, 2741–2750.

Zhang M, Meng X-Y, Cui M, Pascal JM, Logothetis DE & Zhang J-F (2014). Selective phosphorylation modulates the PIP$_2$ sensitivity of the CaM–SK channel complex. *Nat Chem Biol* **10**, 753–759.

Zhang W, Wang D, Liu X-H, Kosala WR, Rajapaksha JS & Fisher TE (2009*b*). An osmosensitive voltage-gated K^+ current in rat supraoptic neurons. *Eur J Neurosci* **29**, 2335–2346.

Additional information

Competing interests

No authors report a competing interest.

Author contributions

The slice preparation, immunochemical identification of neurons, and calcium imaging/uncaging were performed by M.K.K. in W.E.A.'s laboratory. PIP_2 immunochemistry was performed by G.K.C. Calcium imaging/uncaging assistance, software, and data interpretation were provided by J.C.C. All authors contributed to conception and design of experiments. The manuscript was drafted by M.K.K. and edited by all authors. All authors approved the final version of the manuscript, all persons listed as authors qualify for authorship, and all those who qualify for authorship are included.

Funding